CLIMATOLOGICAL ANALYSIS OF METEOROLOGICAL OBSERVATIONS AT THE SUMMIT OF MAUNA KEA

by Sara Couto da Silva, Supervisor Dr. Steven Businger

Dissertation to obtain the degree in Meteorology, Oceanography, and Geophysics

with a specialization in Meteorology (Licenciatura), July 2006

Faculty of Sciences of University of Lisbon, Physics Department

UH MET

UNIVERSIDADE DE LISBOA

Abstract

A comprehensive analysis was undertaken of the meteorological data collected at weather stations operated by the CFHT[1] and UKIRT[1] observatories and located at the Summit of Mauna Kea on the Island of Hawaii. The available data includes the standard variables including wind speed and direction, pressure, temperature and relative humidity or dew point. The CFHT data record extends from 1994 to March 2006 and the UKIRT data record extends from May 1991 until 2005. The objective of the present study is to provide a comprehensive climatological analysis of the available meteorological data at the Mauna Kea summit. The results of the study have broad application in custom forecasting and environmental/ecological studies on Mauna Kea. The climatological analysis includes the following products for each of the variables; monthly means, daily means, maximum and minimum values, diurnal cycle plots, and wind rose charts calculated over the period of record. Climatological results for winter months during El Niño (1997-1998) and La Niña (1998-1999) years are compared with each other and contrasted to the long term mean. A harmonic analysis was undertaken to investigate the character of the annual and semi-annual cycles. A detailed discussion of the implications of the results of the Mauna Kea summit climatology is provided.

---

[1] Canada, France, Hawaii Telescope (CFHT) and United Kingdom Infrared Telescope (UKIRT)

1. Introduction

The summit of Mauna Kea is arguably the best site on Earth for astronomical observations and the capital investment in telescopes on Mauna Kea has exceeded $600 million. The success of astronomical observations on Mauna Kea is strongly influenced by weather conditions (Businger, 2001). Given the concentration of activity at the summit of Mauna Kea, it is perhaps surprising to learn that very little is known about the climatology of the summit region, because no one has as yet undertaken a careful study of the available meteorological data. Understanding the climate of Mauna Kea is useful for the observatories, but it is perhaps more important for understanding the ecology of the summit region. This study is designed to provide insights regarding the climatic variability at the Mauna Kea summit. The main source of data for the climatological analysis are the meteorological observations collected at the Summit of Mauna Kea by two astronomical observatories, CFHT (Canada, France and Hawaii Telescope) and UKIRT (United Kingdom Infrared Telescope). In support of their operations, these observatories collect meteorological data on wind speed and direction, temperature, pressure, relative humidity and dew point. In addition to documenting trends, and extremes, and the average annual and diurnals cycles in weather at the Mauna Kea summit, variation of the climate data at the summit were investigated during el Niño and la Niña events.

CFHT is located at 19° 49’ 30.9” N, 155° 28’ 07.9” W and at 4204 meters of altitude. UKIRT is located at 19° 49’ 20” N, 155° 28’ 13.1” W and at 4194 meters of altitude (see Fig. 1 and Fig. 2). The CFHT telescope is located at a highest altitude of all

telescopes and is isolated from edge factors and surroundings. The UKIRT telescope is located near the 88-inch Hawaii Telescope and has a hill in front of it to the south, which induces some terrain effects. These edge influences do not significantly disturb temperature, pressure, dew point or relative humidity records but can disturb horizontal wind direction and speed.

Hawaii is located in the tradewind belt of the general circulation, which is to say that it lies in a belt of fairly uniform winds blowing from the northeast, emanating from a semi-permanent subtropical high pressure area located to the north of the State. The NE trade winds are a branch of the Hadley cell. The Hadley cell, named after the 17th century scientist who first described it, is a dominant component of the general circulation of the atmosphere that includes convergence and rising motion near ~10° N latitude, southwesterly wind flow aloft, sinking motion in the semi-permanent subtropical high centered near ~30° N latitude and a return flow from the northeast near the surface (NE trades). The Hadley cell is driven by solar radiation and its northward extent is governed in part by the rotation of the Earth (Rosenlof, 1996).

The subtropical high moves with the sun, northward during the summer and southward in winter. The motion of the high results in two seasons recognized by the original Hawaiians, a warm season (Kau) and a cold season (Hoo-ilo). Because Hawaii is at about >3000 km far away from a continental landmass, the ocean works as a giant thermostat to moderate temperature and humidity changes throughout the year. Hawaii impacted by storms and fronts (in winter) but the temperatures don't change as much as they would over the continent, because the air that reaches Hawaii has traveled for a very long distance over the ocean and has been moderated.

In addition to latitude and ocean, which define Hawaii's weather and climate, the Island of Hawaii has topographic diversity that produced large contrasts in local climates. Mauna Kea is one of two mountains on the Big Island. The summit of Mauna Kea has an altitude of 4205 meters and is classified as peri-glacial climate or tundra[2] (Preston E. James, 1922), because the mean monthly temperature along the year is below 10° C and the rainfall is scant. Mauna Kea and Mauna Loa form a barrier to the wind. Although orographic precipitation is prevalent in the lowlands of the island, at the higher altitudes (>2500 m) rainfall is infrequent, because of the prevailing tradewind inversion that caps moisture below. Above the tradewind inversion clear skies, low humidity, and cool temperature are present most of the time, making Mauna Kea an outstanding location for Earth-based astronomy.

2. Data and Methodology

2.1. Data

CFHT data were collected every ten minutes from 1 January 1994 through December 2002 and every five minutes from January 2003 through March 2006. CFHT data do not include dew point measurements, and there are no pressure observations for the years of 1994 and 1995. The UKIRT data used in this study were recorded every fifteen minutes from May 1991 – through December 2005.

---

[2] According to Koppen Climate classification of the Island of Hawaii, which considers temperature mean variations and rainfall mean variations along the year.

The meteorological data sets from both observatories were carefully evaluated for quality. The errors were of several types, such as non-physical values for a certain variable, constant value for a long period (days or months) and values that were out of the range for the variable in question.

Examples of non-physical values include negative wind speeds or relative humidity. Pressure data included, frequently, values equal to zero hPa and a constant high value for a long period (CFHT - July 1998). Temperature and dew point data had low constant negative values for a long period (UKIRT - September 2004 until April 2005). Relative humidity data had negative and zero values included in the initial data lists.

2.2. Data quality control

Initially, the data were separated by years and months and were plotted without any quality control. The first validation consisted of plotting all data along the year and identifying values that were inconsistent with the variation range of the variable. The second validation consisted of plotting the variables by month in order to evaluate odd values. In this case, these odd points were compared to weather records available on Internet for that particular date. The weather website available for Hilo, Big Island, served as a background meteorological record that helped in validating the data. After validating all data, the data were separated by years and months and re-plotted. The final validated data are shown on Table 1.

Meanwhile there are plots that required pairs of data, such as wind rose charts or scatter plots. The input data to build a wind rose plot are wind direction and speed as pairs of data. To plot wind rose charts the wind data were validated separately. In this

case, instead of considering wind speed and wind direction values as independent measurements, they were validated at the same time and as pairs of values. The table for valid wind values as a set of wind direction and wind speed is the reunion between the valid dates of wind speed and wind direction data reported in Table 1.

The objective of a scatter plot is to relate pairs of variables. These plots were made for wind speed and pressure, pressure and temperature, and wind speed and temperature. All pairs of values mentioned above were validated by the same method as used to validate the wind data used in wind rose charts.

2.3. Methodology

The climatological analysis includes the following products for each of the variables; monthly means, daily means, maximum and minimum values, diurnal cycle plots, and wind rose charts calculated over the period of record. Standard deviation was computed for each variable. Standard deviation is a statistical parameter that measures the excursion of the values in relation to their mean value (Eq. 1).

$$\sigma = \sqrt{\frac{1}{n}\sum_{i=1}^{n}\left(x_i - \bar{x}\right)^2} \qquad (1)$$

Where n is the total number of points and i is each point.

Harmonic Analysis constitutes a useful tool to study periodic variations of a meteorology variable. Its mathematical definition sustains that a function (in this case a curve) can be represented as a series of trigonometric functions, as in Fourier series. Each harmonic (in this study first and second harmonics) has correspondent amplitude and

phase values, which provide information about the annual cycle of the variable (Kristina Kyrkila, 1989). A high amplitude value for the first harmonic (strong first harmonic) means a strong annual variation for the variable while a high amplitude value for the second harmonic (strong second harmonic) means a strong semi-annual cycle. Harmonic analyses of pressure, temperature, and wind speed annual variations were calculated (Eq. 2)

$$X_t = \overline{X} + A_k \cos\left(\frac{2\pi kt}{n} - \varphi_k\right) \tag{2}$$

In which X_t is the monthly mean calculated series for each t, t is the considered month, $\overline{X}$ is the yearly mean, A_k (Eq. 3) is the amplitude for each k harmonic, n is the total number of points (12 months or 12 points in this case) and φ_k is the phase at each k harmonic.

$$A_k = \sqrt{C_k^2 + S_k^2} \quad \text{and} \quad \begin{cases} C_k = \dfrac{2}{n}\displaystyle\sum_{t=1}^{n} x_t \cos\left(\dfrac{2\pi kt}{n}\right) \\ S_k = \dfrac{2}{n}\displaystyle\sum_{t=1}^{n} x_t \sin\left(\dfrac{2\pi kt}{n}\right) \end{cases} \tag{3}$$

is the amplitude at each k harmonic.

The objective of a scatter plot is to relate pairs of variables and to conclude about their possible linear relationship. These plots were made for wind speed and pressure, pressure and temperature and wind speed and temperature. A scatter plot is a graphic

representation in which the y variable is plotted as a response of the x variable. The linear relation between the two variables is given by their correlation coefficient. Correlation coefficient varies between -1 and 1 suggesting a high negative linear relation in the first case and a high positive relation in the second. When there is no linear relation the correlation coefficient is equal to zero and the variables are not linearly related to each other.

Wind rose plots are commonly used to study horizontal wind vector data. Wind rose is a polar representation of the frequency of the wind flow as a function of wind direction for a particular location and for a certain period (short period - month or long period - year or set of years). Several concentric rings constitute this plot and it is divided in sixteen quadrants of twenty-two and a half degrees each. The north, east, south and west directions rotate in clockwise direction.

3. Analysis Results

The results of the analysis of data from CFHT and UKIRT are very similar, except for the wind data. CFHT recorded data is nearer the true summit of Mauna Kea; therefore, for the sake of brevity, the results presented in this section are primarily from the analysis of CFHT data.

3.1 Surface Pressure

Surface pressure has a well-defined annual cycle with a maximum in August (P = 616.19 hPa) and the minimum in February (P = 613.34 hPa). Pressure increases from

February to August and decreases after August (Fig. 3). These pressure variations are consistent with the motion of the sub tropical anticyclone during the year and its position relative to Hawaiian Islands. During summer months, the North Pacific anticyclone is strongest, reflecting an enhanced Hadley circulation (Rosenlof, 1986). The high weakens gradually as the sun moves south of the equator, and pressure decreases during the fall months. During winter, the westerlies shift southward bringing synoptic weather systems (cold fronts and kona lows) that result in a decrease of pressure values during these months.

The annual cycle is confirmed by calculating the first and second harmonics for pressure. The first harmonic or annual cycle amplitude is much higher (A = 1.6 hPa) than the second harmonic or semi annual cycle (A = 0.24 hPa) (Fig. 4). Pressure has an annual amplitude of 3.35 hPa and a low standard deviation coefficient (σ = 11.58 hPa), which means pressure values during the year do not vary much. Because of the impact of winter storms, the amplitudes of daily pressure variations are larger in winter, when the lowest mean values are observed, than in summer, when the highest mean values are observed (Fig. 5 and Table 2).

Pressure has a semi-diurnal cycle with a 12-h period that is a consequence of the solar tide near the tropics (Fig. 6) (Aiguo Dai and Junhong Wang, 1999). The solar tide in tropical regions is the dominant diurnal forcing term, and is larger than other forcing terms such as the lunar tide or soil heating. The solar tide behaves as an internal gravity wave and results in two maxima and two minima each day. The first maximum occurs near 10 AM HST and the second one near 10 PM, the first minimum occurs near 4 AM and the second one near 4 PM. This semi diurnal cycle for pressure is maintained

throughout the year, but the amplitude changes with time of year. The difference between the first maximum and minimum is larger than the difference between the second maximum and minimum. This observation is a consequence of the superposition of other forcing terms (lunar tide, soil heating and others) with different periods (T = 8 h or T = 24 h). The first semi-diurnal amplitude varies during the year, decreasing from winter (A = 2.21 hPa) to summer (A = 2.01 hPa). This result is consistent with the daily mean pressure variation, which exhibits a higher value in winter months than in summer months.

3.2. Temperature

Temperature, like surface pressure, displays a well-defined annual cycle with a maximum in September (4.47 °C) and a minimum in February (0.28 °C) (Fig. 7). The fact that the maximum value occurs late in summer (September) and the minimum value occurs late in winter (February) is a reflection of the seasonal lag, the difference between the solar forcing cycle and the annual temperature cycle at a point, whose amplitude in time is know to decrease from the equator to the poles. Seasonal lag observed in Hawaii is largely because of the large heat capacity of the surrounding Pacific Ocean.

Temperature values are not quite as sinusoidal since June has higher temperature values than July and August. Comparison of the first and the second harmonic amplitudes confirms the dominance of the annual cycle (Fig. 8). The first harmonic value (A = 2.22 °C) is much higher than the second harmonic amplitude (A = 0.26 °C). The standard deviation of the mean temperature values is small, indicating that temperature values are fairly constrained throughout the year.

The daily mean temperatures show little variation throughout the year, but the absolute amplitude (difference between the absolute maximum and the absolute minimum temperatures) shows a larger annual variation (Fig. 9). The greatest absolute amplitude is in January and the smallest occurs in September, primarily a reflection of lower minimums during winter (Table 3).

Temperature has a diurnal cycle with a period of 24 hours, a maximum at 1:00 PM HST and a minimum at 5:00 AM (Fig. 10). The timing of the maximum and minimum air temperatures reflects the response of the surface to solar radiation and turbulent exchange of energy in the surface layer. The diurnal pattern has the same shape for all months of the year, but the diurnal amplitude is bigger in summer (4.46 °C) than in winter (3.52 °C), a reflection of the greater solar forcing in summer.

3.3 Relative Humidity

Relative humidity (RH) is roughly constant throughout the year over Mauna Kea. The annual mean RH is 36% and it has an annual range of 11% (Fig. 11). The highest monthly mean RH occurs is November (41%) and the lowest occurs in April (30%). The standard deviation of the monthly means is 3.1%, which is rather small, indicating that monthly mean RH values do not vary much from month to month. The relatively low values for relative humidity are a consequence of the summit's altitude, which places the summit in the free troposphere, above the prevailing trade-wind inversion altitude (around 2000 m). Typically, warm moist air that advects from the ocean, is forced to rise reaches saturation, and condenses well below the summit. Although conclusions regarding rainfall cannot be made from relative humidity values alone, the low mean

values for relative humidity are consistent with the classification of Mauna Kea's climate as arid.

Daily mean relative humidity observations remain near the annual mean throughout the year (Fig. 12). However, daily values of RH do range from 2% to 100%, reflecting the impact of storm systems bringing moist air to the summit, and strong subsidence events bringing dry air from near the tropopause to the summit. Daily maximum RH >80% indicate that precipitation is possible during any given month of the year.

RH has a weak diurnal pattern that varies in amplitude during the course of the year (Fig. 13). The diurnal cycle is not as well defined in winter as in summer. The August diurnal cycle in RH has an amplitude of 11%, whereas in December the diurnal cycle is masked by other oscillations and the maximum amplitude is less than 5%. In summer, the pattern is similar to that of temperature (Fig. 13), with a maximum near 3 PM HST and a minimum near 6 AM. This similarity in summer is somewhat surprising, since the amount of water in the air at saturation (RH = 100%) is a sensitive function of the temperature, which in turn is strongly forced by solar radiation. Thus, assuming the specific humidity is nearly constant during the day, the RH should track exactly out of phase with the temperature curve, falling off during the afternoons and rising in the early morning. The fact that this is not the case implies that the specific humidity is not constant, but increases significantly during the afternoon in response to moist air rising with the trade-wind inversion, being forced to the summit level by kinetic energy in the flow.

The complex diurnal pattern observed in winter is more difficult to explain. In the absence of a strong diurnal change in the level of the trade-wind inversion, the pattern may result from a superposition of the inverse relationship of RH and temperature and the tendency for instability to be greater in the afternoon, allowing moisture to show a maximum during the afternoons.

3.4. Dew Point (UKIRT)

The dew-point temperature, or dew point, is the temperature to which the air must be cooled, isobarically and maintaining the same amount of moisture, to reach saturation (relative humidity = 100%). For cloud condensation to occur the temperature of an aerosol particle must reach the dew point. The monthly mean values of surface dew point at UKIRT are below freezing for all months of the year (Fig. 14). The monthly-mean values are significantly below the monthly-mean temperatures, consistent with the low mean RH values at CFHT. The annual mean value of the dew point is -15.5°C and the standard deviation is small (2.1°C), indicating that the values do not vary much from year to year. The annual range of dew point is 5.5 °C, the coldest month being December (-18.5°C) and the warmest is August (-13°C).

Some of the noisiness seen in the daily data reflects the relatively short data record (Fig. 15). Dew point behavior is in phase with temperature behavior most of the time and daily dew point variations are practically the same during the year. The highest values for dew point occur during summer months and the lowest values occur during the winter.

The diurnal cycle of dew point is similar to the diurnal cycle of temperature. The period of the cycle is 24 hours, the maximum occurs near 3 PM HST and the minimum occurs at 5 AM (Fig. 16). All months of the year exhibit the same pattern, but the diurnal amplitude is larger in summer (9.2°C) than in winter (6.6°C). It is interesting to note that diurnal dew point variation is greater, even in February, than annual dew point variation. The fact that dew point and temperature values are in phase may be a reflection of the decrease in stability associated with afternoon heating as discussed previously.

3.5. Mixing Ratio (UKIRT)

Mixing ratio is defined as the ratio of the mass of water vapor in the air to the mass of dry air (grams of H_2O per kilogram of dry air). The mixing ratio over Mauna Kea is generally very low, with an annual mean value of 2.4 g/Kg and a standard deviation value of 0.4 g/Kg. The values vary from a minimum in April (1.8 g/Kg) to a maximum in August (3.1 g/Kg) (Fig.17). Mixing ratio has a well-defined diurnal cycle with a period of 24 hours (Fig. 18). The maximum peak occurs around 3 pm (similar to temperature and dew point) and the minimum occurs around 2 am. Diurnal amplitude changes during the year, being higher in August (1.8 g/Kg) than in February (0.8 g/Kg). This variation in amplitude is in agreement with temperature and dew point amplitude variations.

3.6. Wind

Surface wind observations were evaluated using two different approaches, (i) wind speed data were analyzed independent of directional data and (ii) wind rose charts that combine the speed and direction information were constructed. The results for CFHT

and UKIRT are different in both studies. UKIRT might have some surrounding effects and edge influences that alter wind speed and direction values. The proximity to other observatories may produce a wind direction shift and a wind speed decrease in mean value.

Wind patterns in the free troposphere over the summit of Mauna Kea reflect shifts in the position of the subtropical anticyclone and the midlatitude westerlies in response to the annual cycle of the position of the sun. During the warm season, the depth of the anticyclone increases, bringing winds with an easterly component to the summit. During the cool season, the polar vortex expands suppressing the anticyclone, and bringing stronger winds with a westerly component to the summit. Winds in the surface layer of the summit are subject to deflection and turbulent stress through interaction with the topography of the summit area and the presence of observatory structures.

CFHT Winds

At CFHT, the wind speed has an inverted annual cycle, with the strongest winds occurring in January (10.2 m s^{-1}) and the weakest winds in September (~5 m s^{-1}) (Fig. 19). Looking to annual wind rose chart (Fig. 20) it is easy to see that there are two prevailing directions for wind to blow from in this region, east and west. If the wind rose is divided into winds with a westerly component and winds with an easterly component, each side encompasses roughly half of the time. Of the total, only 10% of the wind is strong (> 10 m s^{-1}) and 18% of the time the wind is due easterly. Due easterly wind is strong ~ 4% of the time. Winds with a westerly component have a frequency of ~30% (12% are due westerly), with wind speeds > 10 m s^{-1} 11% of the time.

During winter the wind over Hawaii blows predominately from west because the influence of subtropical anticyclone is less and the Aleutian low-pressure center extends towards equator, bringing with it fronts and rain bands (Gunnar I. Roden, 1980). The wind in January (Fig. 21) is from NW to SW 51% of the time and exceeds 10 m s^{-1} nearly a third of the time. Winds have an easterly component 22% of the time.

During the warm season, a strong subtropical anticyclone is located north of the Hawaiian Islands and exerts a strong influence on the Island weather. As a result, northeast trade winds are prevalent during summer months and extend to the summit. Wind speeds at Mauna Kea decrease to their lowest mean value in September, as the strength of the anticyclone wanes and the stronger westerlies aloft have not developed yet. The wind rose chart for September shows that the wind direction in has an easterly component 53% of the time and strong winds are infrequent (< 5%) (Fig. 23).

May is a transition month between the cool and warm seasons. The May wind rose chart (Fig. 22) reflects this transitional nature with the frequency of easterly winds in balance with the frequency of westerly winds.

Daily variations in wind speed are larger in winter (December through March) than in summer (June through September) (Fig. 24). The diurnal cycle in wind speed is very weak or nonexistent, with amplitude of < 1 m s^{-1} in winter and summer (Fig. 25). Moreover, the timing of the diurnal pattern of maxima and minima is inconsistent throughout the year.

UKIRT Winds

Although the winds at UKIRT show similarities to those at CFHT, there are also significant differences that are attributable to local variations in topography and a slightly lower altitude, resulting in a different exposure. The yearly variation of UKIRT winds is similar to that of CFHT. The highest winds are observed during the winter, with a maximum in January (7 m s^{-1}), and the lowest winds are observed during summer, with a minimum in September (~2 m s^{-1}) (Fig. 19).

The amplitudes of the first and the second harmonics of the wind speed time series confirm that the wind speed at UKIRT has a well-defined annual cycle. The first harmonic amplitude (A = 1.7 m s^{-1}) is larger than the second harmonic amplitude (A = 0.6 m s^{-1}).

The mean winds at UKIRT are consistently lower than at CFHT, reflecting the impact of the lower altitude and differing exposure. The annual mean value is 3.8 m s^{-1} and the annual range of variation is 4.7 m s^{-1}, which is of the same order of magnitude as that of CFHT. Wind rose charts show a lot of variation for January (Fig. 21), May (Fig. 22) and September (Fig. 23). The absence of winds from the northeast quadrant during these months is indicative of local blocking of the wind by the proximate observatory structure, which also produced variability in the wind direction through turbulence.

The diurnal cycle for wind speeds for February and August are out of phase and the amplitude is weak year round, < 1 m s^{-1} (Fig. 25). During February, the maximum occurs near 5 AM and the minimum occurs near 12 PM, whereas in August the maximum is at 3 PM and minimum is at 5 AM.

3.7 Snowfall proxies

The available data for this study did not included rainfall observations; therefore, it is not possible to study directly the climatology of rainfall and/or snowfall at the summit of Mauna Kea. However, conditions suitable for the occurrence of frozen precipitation (e.g., snowfall) at the summit, such as available moisture and temperatures below freezing for a number of hours, can be investigated to estimate the frequency and annual variability of the occurrence of snow. In this way, we can create a snowfall proxy. In this study if the hourly mean temperature was below freezing ($T < 0°C$) and relative humidity was higher than 80% ($RH > 80\%$), and these hourly mean values were observed for ≥ 4 hours, then we note the occurrence of a snowfall event.

The snowfall proxy 1 chart (Fig. 34 a)) shows that these conditions were observed in January more often than in any other month (6 events during the average January). The snowfall occurrences are a function of both relative humidity and temperature and the months at which the snowfall events are the most in number correspond to the months during which the temperature is a minimum (January, February and March) or the relative humidity is a maximum (November).

September has the least events, with zero events. The months during which the chance of snow is least are months with warm temperatures (September, June, August) and low relative humidity (April, December or October). It is curious to observe that July, a month with temperatures, has several events, because of very high relative humidity. Those with experience at the summit, however, note that during the summer accumulation of snow is rare.

A snowfall proxy 2 was undertaken in order to compare the results with the first proxy results. In this proxy, mean hourly temperature and precipitable water were considered. In this study if the hourly mean temperature was below freezing ($T < 0°C$) and precipitable water was higher than 4 mm ($PW > 4$ mm), and these hourly mean values were observed for ≥ 4 hours, then we note the occurrence of a snowfall event.

The snowfall proxy 2 chart (Fig. 34 b)) shows that these conditions were observed in March more often than in any other month (6 events during the average March). The snowfall occurrences are a function of both precipitable water and temperature and the months at which the snowfall events are the most in number correspond to the months during which the temperature is a minimum (January, February and March) or the precipitable water is a maximum. There is not a study made regarding precipitable water monthly means. Precipitable water values were received two days before the conclusion and presentation of this work and so the values were uniquely used to induce a snowfall proxy.

September has the least events, with zero events. The months during which the chance of snow is least are months with warm temperatures (September, June, August). Meanwhile precipitable water is related to relative humidity and the months at which relative humidity is the highest should be related to the months at which precipitable water is the greatest. But, in the absence of a detailed monthly study of precipitable water no conclusions of snowfall proxy can be done regarding precipitable water values along the year.

Comparing both proxies, the second one is more reliable than the first specially because the decrease of occurrences (the summit is considered as arid) and the

distribution throughout the year, which agrees with the second minimum monthly temperature, value during the year (March) and with the maximum monthly mean temperature values (September and June). It is clear that considering precipitable water as an initial condition to a snowfall occurrence is more reliable than considering relative humidity values above 80 %, since it is known that relative humidity can be above 80 % and the particle can not condensate to precipitate as snow.

4. El Niño and La Niña

El Niño and La Niña phenomenon are two phases of a Pacific-scale ocean-atmosphere interaction known as El Niño Southern Oscillation (ENSO). ENSO consists of the oscillation that occurs in a standardized mean difference in sea-level pressure between Tahiti (T) and Darwin (D). The difference between these two sites drives a circulation, known as the Walker cell, which extends from the west side to the east side of the Pacific Ocean. Deviations in the mean value of the pressure difference (T-D) signal the onset of an El Niño or a La Niña. The Walker cell produces easterly winds driving an easterly ocean current along the equator. The Coriolis force acting on this easterly current produces upwelling and cool sea-surface temperatures (SSTs) (Bob Henson and Kevin Trenberth, 1998).

During El Niño events, the strength of the Walker cell diminishes and the flow across parts of the equatorial Pacific reverse from easterly to westerly, resulting in downwelling and warm SSTs. The southern oscillation index (SOI) is an index that tracks the difference between the pressures at the two distant sites, T and D.

$$SOI = T - D$$

If T is lower than usual and D is higher than usual, the SOI will be negative and an El Niño is triggered. The consequences of El Niño in Pacific Ocean are a strengthening of ITCZ (Inter Tropical Convergence Zone) over the central Pacific, and a shift of the SPCZ (South Pacific Convergence Zone) equator ward, resulting in enhanced convection over the central equatorial Pacific. The result of these changes over Hawaii includes increased subsidence and winds at the level of the summit shifting northeastward.

The opposite situation is La Niña, which occurs when the pressure at Tahiti is higher than usual and the pressure over Darwin is lower than usual, causing SOI to be positive. The pressure gradient is higher than normal and the trade winds are stronger than usual. This increase in trade-winds intensity enhances the easterly ocean current along the equator; as a result, the upwelling of bottom waters is stronger and more persistent than in normal years. The consequences of La Niña include enhanced convection over western Pacific Ocean and diminished convection over the central equatorial Pacific. Over Hawaii, these changes result in enhanced westerlies aloft during winter and an increase in clouds and moisture over the summit.

In this study, the difference in seasonal mean value between ENSO (El Niño and La Niña) and normal values were computed for the four winter months, December through March. Winter months were chosen because the impact of ENSO is most pronounced over Hawaii in winter. During the period of available data, the year 1997/98 was an El Niño year and the following one (1998/99) was a moderate La Niña year.

The 1997/98 El Niño was considered one of the strongest of the last century, producing a persistent drought in Hawaii and record-setting temperatures globally in February. An enhanced Hadley circulation over the central tropical Pacific during this event caused the winter mean pressure to increase by 1.7 hPa (Fig. 26). The winter mean temperature increased 2.5 °C (Fig. 27), whereas the mean winds were weaker, decreasing by 2 m/s (Fig. 28). The wind rose during El Niño conditions show a slight increase in winds with a westerly component (2% more than in normal situation), the frequency of strong winds decreased (Fig. 31). The winter mean relative humidity showed the greatest impact, with a decrease of nearly 20% (Fig. 29). Similarly, the mean dew point decreased (-6.6) °C (Fig. 30) and mixing ratio decreased (-1.05) g/Kg (Fig. 30). Two tables are provided in which both mean variations for winter months (December through March) and each month variation (December, January, February and March) and compared to the mean values for the winter situation and each winter month in the average results (Table 5 – CFHT and Table 5 – UKIRT).

The 1998/99 La Niña was moderately strong and the deviation of the variables from normal was much smaller than during the preceding El Niño. The mean winter pressure and winds were nearly normal (Fig. 26), whereas the mean temperature was ~ 1 °C colder than normal (Fig. 27). The direction of wind changed substantially from generally westerly, the common pattern in winter, to predominantly easterly directions, while strong winds were 13% more frequent than normal (Fig. 32). Relative humidity decreased slightly in 3.719% (Fig. 29) and dew point temperature increased in mean value in 0.52 °C (Fig. 30) while mixing ratio increased too in 0.1 g/Kg (Fig. 30).

During the 1997/98 El Niño and the 1998/99 La Niña, the snowfall proxy 1 produced fewer events than normal during the winter months, December through March. The El Niño winter had 3 events, while the La Niña winter had 13 events, compared with 18 events in an average year. During El Niño a significant decrease in relative humidity occurred and temperature in increased by ~ 2 °C, thus the decrease in proxy snowfall events was expected.

The snowfall proxy 2 produced results more consistent with the observed variation in the variables during ENSO years during winter. The El Niño winter had 1 possible event, while the La Niña winter had 15 events compared with 16 events in the average year. El Niño winter results agree in both proxies, and it is clear to observe that the available precipitable water must have decreased substantially during the winter months of this year while temperature increased, and so the decrease in probable events was expected. La Niña winter produced a similar number of snowfall occurrences when compared to the average year but during December 1 more event was possible to occur and in January 5 more events were probable to happen. January increase in snowfall events is observed in both proxies during La Niña year and a decrease in snowfall events is observed in both proxies during El Niño year. Second snowfall proxy present more reliable results than the first snowfall proxy because in La Niña year there were not significant changes in values compared to the regular situation, which agrees with the variation of the variables, compared to climatology results.

5. Investigation of correlations between variables

One of the objectives of climatological studies is to understand the relationships between the observations. If variables are related to each other, the behavior of one variable can be used to predict the behavior of the other. An easy way to look for such relationships is by producing scatter plots of pairs of variables, e.g., pressure and temperature, pressure and wind speed, and temperature and wind speed. The method of least squares can be used to gage the degree of correlation, assuming a linear relationship. If the correlation coefficient has a value above 0.5 (-0.5) the variables are said to correlate positively (negatively) and a line can be drawn that represents the best fit to the data points. If correlation coefficient is below 0.5 or -0.5, the variables do not correlate and no linear relationship can be inferred.

Pressure and temperature do correlate at the summit during winter and do not correlate during summer (see Figs. 35 and 36). The correlation coefficient during winter is equal to 0.62. The equation is for temperature as a function of pressure is

$$T = 0.631P - 387$$

The correlation between temperature and pressure decreases from winter months when it is greatest to the summer months when the correlation vanishes. The scatter plot for July is representative of a lack of a relationship between the two variables.

Pressure and wind speed are two important variables in meteorology studies. Large pressure gradients are associated with strong winds, but in this study, we are limited to comparing the variables directly, and not their gradients. Therefore, it is not surprising to see that the variables are uncorrelated in March or in July (Figs. 37 and 38).

Effectively these two variables are uncorrelated or very weakly correlated, with the highest correlation coefficient observed in March (-0.49) remaining below the threshold of 0.5. Temperature and wind speed are even less correlated. The highest value of the correlation coefficient was observed in May, with a value of -0.27 (Fig. 39).

6. Conclusions and Discussion

Given the uniqueness of environment at the summit of Mauna Kea and the concentration of scientific activity there, it is surprising that so little is known about the climatology of the summit area. Understanding the climate of Mauna Kea is clearly critical for understanding the ecology of the summit region. In this section, the conclusions resulting directly from the analysis of meteorological observations made at CFHT and UKIRT are presented first, followed by a discussion of the implications of these conclusions. The conclusions are organized loosely into groups relating the conclusions to aspects of the geography of Mauna Kea.

Features associated with the latitude of Mauna Kea

- Semi-diurnal cycle in pressure is a consequence of solar tide.
- Seasonal lag in temperature is associated with latitude and ocean environment.
- Annual amplitude in monthly mean temperature ($\Delta T = 4.75$ °C) is similar to its diurnal amplitude ($A = 4.46$ °C).

Features associated with the altitude and orography of Mauna Kea

- Monthly mean Temperature is < 5 °C, and pressure is low, ~ 615 hPa.
- Relative humidity is nearly constant throughout the year, the mean value is low ~ 36 %.
- Mean value of the dew point temperature is more than 10 °C below that of the temperature.
- Mean value of the mixing ratio is low, w ~ 2.4 g/Kg
- Complex but weak diurnal cycle in wind speed and direction.
- Rainfall is infrequent (relative humidity and mixing ratio are low and dew-point depression is large).

Changes associated with the annual cycle of solar forcing

- Climate can be roughly characterized by two seasons: May through September – warm season (Kau), and October through April – cool season (Hoo ilo)
- May - September: temperature and pressure have their highest annual values, wind speeds are weakest and the wind blows predominantly from the east
- October - April: temperature and pressure have their lowest annual values, wind speeds are strongest and blow from predominantly from the west
- Temperature, dew point, relative humidity and mixing ratio diurnal variations are larger during the warm season than in the cool season.
- Changes in wind direction (east and west) result from changes in the general wind circulation in the subtropics, which follows the annual cycle in the position of the sun.

Conclusions related to ENSO

- During the El Niño year, the winter mean value of temperature was higher than usual, relative humidity was substantially lower, dew point was lower, winds were weaker, and rainfall was even more infrequent.
- During the La Niña year winter mean value of temperature was lower than usual, relative humidity was slightly lower, dew point was higher, wind was stronger and trade winds prevailed and rainfall was more frequent.

Discussion

The latitude, the altitude, and the orography of the summit of Mauna Kea along with it remote island location all help to define its local climate. The subtropical latitude produces typical tropical variations in the behavior of the variables, such as the semi-diurnal pressure response to the solar tide. The ocean environment produces a notable seasonal lag in temperature, with the highest temperatures in late summer and the lowest temperatures happening late in winter. Diurnal variations in temperature are similar in magnitude as the annual temperature variation, typical of the tropics since the annual variation in solar radiation is small.

The summit of Mauna Kea is at ~4 km altitude resulting in low mean pressure values (~615 hPa) and low mean temperatures (~5 °C). Low relative humidity and infrequent precipitation are also a consequence of the altitude of the summit and subsidence associated with the Hadley circulation over the central Pacific.

During El Niño winters, December through March, mean temperatures are warmer than average, relative humidity is substantially lower, and rainfall is below normal. Moreover, the wind is weaker, and more westerly.

This study provides a starting point for understanding the atmospheric environment of Mauna Kea, and demonstrates tangible progress in analyzing meteorological data collected at two summit observatories, CFHT and UKIRT. However, there is considerable opportunity for additional work to more fully understand this interesting and important ecosystem.

Future work

This subsection outlines some approaches to synthesizing observations and numerical model investigations to provide further insights into the climatic variability, ecological conditions, and transport of biota to the Mauna Kea summit.

Since the data record for the summit of Mauna Kea is limited (1992-2006 in digital form), there are two approaches to extending the climate record to more fully characterize the meteorological variability and probe questions relating to inter-decadal variability and the potential impact of predicted climate change. The first is to use the longer data record available from Mauna Loa to extend the study of climate variations at altitude on the Island of Hawaii. The period for which both sites have data can be used to establish the relationship between the two sites. This relationship can then be used to generalize the climate changes observed at Mauna Loa, over its longer record, to Mauna Kea.

The second approach is to use a high-resolution numerical weather prediction model[3] to run extended "daily" simulations using as initial conditions the reanalysis data set available over the central north Pacific region and extending back to 1950. The high-resolution model includes the complex terrain of the island, which is absent in the reanalysis data, and therefore the model is able to reproduce the sharp gradients in clouds, moisture and winds that characterize the island's climate. The model output will be used to investigate the standard meteorological variables. Biases in the model output will be corrected using the summit observational climatology that is now available. In addition to investigating in the model output the average annual and diurnals cycles in weather at the Mauna Kea summit, trends, extremes, and the variation of the climate across the summit during past decades will be studied. The resulting products will then be compared to products constructed from observed data collected at Mauna Loa and Mauna Kea.

Using a similar approach, future changes in the microclimate of the summit region during the coming century can be studied by using climate model output to initialize our high-resolution weather model. In this way, the impact of global warming on the level of the trade-wind inversion, the direction and strength of the winds, and temperature and moisture characteristics can be anticipated for the coming decades.

Source regions and transport of food for the Wekiu bug will be investigated using a combination of observed and modeled winds with the aid of a trajectory model. In particular, the Hybrid Single-Particle Lagrangian Integrated Trajectory (HY-SPLIT)[4] model will be used to produce an accurate estimate of the concentration and dispersion of

---

[3] for background on our weather modeling program see: http://mkwc.ifa.hawaii.edu/models/index.cgi

[4] for background on dispersion modeling see: http://imina.soest.hawaii.edu/MET/Faculty/businger/poster/vog/

food particles for the Wekiu bug. Wind fields and thermodynamic data from the high-resolution output of our operational weather prediction model[1] will be employed as input for the HY-SPLIT model.

A combination of satellite remote sensing, surface-based observations, and food particle samples collected during site visits to the field will be used to validate the high-resolution model simulations of summit weather and also to validate the trajectory and dispersion model predictions of food particle distribution.

Acknowledgments

This report is the result of an internship undertaken in Meteorology Department, University of Hawaii at Manoa, Oahu, Hawaii. Dr. Steven Businger, who showed great availability all the time to help, supervised this internship. The author thanks Dr. Steven Businger the acquired knowledge and the warm and friendly reception. The author thanks to her family the possibility of undertaking this internship out of Portugal providing financial support and the shared love while she was far away. The author thanks her friends, in Portugal and in Hawaii (the new ones), for participating enthusiastically in her life. The author thanks Prof. Pedro Miranda too for allowing this internship as a part of Meteorology degree and for being available to talk about it when it was being settled.

7. References

Aiguo Dai, Junhong Wang, 1999: Diurnal and Semi-Diurnal Tides in Global Surface Pressure Fields. Journal of Atmospheric Sciences: Vol. 56, no. 22, pp 3874 – 3891.

Bob Henson, Kevin E. Trenberth, 1998: Children of the Tropics: El Niño and La Niña.

Businger, S., R. McLaren, R. Ogasawara, D. Simons, and R.J. Wainscoat, 2001: Starcasting. *Bull. Amer. Met. Soc.*, **83**, 858–871.

Caruso, S. and S. Businger, 2006: Synoptic climatology of subtropical cyclogenesis. *Wea. and Forecasting*, **20,** 193-205.

Cherubini, T., S. Businger, C. Velden, and R. Ogasawara, 2006: Assimilation of satellite derived winds in mesoscale forecasts over Hawaii. *Mon. Wea. Rev.*, **134**, 2009-2020.

Cherubini, T., S. Businger, R. Okasawara, and R. Lyman, 2006: Modeling turbulence and seeing over Mauna Kea. Submitted to J. Appl. Meteo., In review.

G. C. Asmani, 1968: Directness of Hadley Cell is in Question. Journal of the Atmospheric Sciences: Vol. 25, no. 5, pp 935 – 935.

Gunnan I Roden, 1980: On the Subtropical Frontal Zone of Hawaii during Winter. Journal of Physical Oceanography: Vol. 10, no. 3, pp 342 – 362.

Karen H. Rosenlof, Duane E. Stevens, John R. Anderson and Paul E. Ciesielski, 1986: The Walker circulation with observed Zonal Winds, a Mean Hadley Cell and Cumulus Friction. Journal of Atmospheric Sciences: Vol. 43, no. 5, pp 449 – 467.

Kristina I. Kirkyla and Sultan Hammed, 1989: Harmonic Analysis of the seasonal cycle in Precipitation over the United States: a comparison between observations and a general circulation model. Journal of Climate: Vol. 2, no. 12, pp 1463 – 1475.

Morrison, I. and S. Businger, 2001: The synoptic structure and evolution of a kona low. *Wea. and Forecasting*, **16**, 81-98.

Preston E. James, 1922: Koppen's classification of Climates: a Review. Monthly Weather Review: Vol. 50, no. 2, pp. 69 – 72.

Tables:

Table 1 : Available data after validation

variable	CFHT data	UKIRT data
wind speed	Jan 1994 - July 1994 March 1995 - March 2006	May 1991 - Dec 2005
wind direction	Jan 1994 - July 1994 Jan 1995 - March 2006	May 1991 - May 2001 Oct 2001 - Dec 2005
pressure	Jan 1994 - March 2006	Jan 1995 - May 2001 Aug 2001 - Dec 2005
dew point	not available	May 1991 - Sep 2004 May 2005 - Dec 2005
temperature	Jan 1994 - March 2006	May 1991 - Sep 2004 May 2005 - Dec 2005
relative humidity	Jan 1994 - March 2006	May 1991 - Dec 2005

variable	CFHT data	UKIRT data
wind (wind speed and direction)	Jan 1994 - July 1994 March 1995 - March 2006	May 1991 - May 2001 Oct 2001 - Dec 2005

Table 2 Pressure Analysis Results

		CFHT	pressure in hPa				
	ave p	mean of max (A)	mean of min (B)	abs max (AA)	abs min (BB)	A - B	AA - BB
Jan	613.5	615.2	611.8	621	600.1	3.4	20.9
Feb	613.3	614.9	611.7	620.2	599.4	3.3	20.9
Mar	613.4	615.1	611.8	620.3	598.0	3.3	22.3
Apr	614.8	616.3	613.2	620.3	607.8	3.0	12.5
May	615.5	616.8	613.9	621.3	607.3	2.9	13.97
Jun	616.3	617.4	614.9	622.0	610.7	2.6	11.3
Jul	616.5	617.7	615.1	622.4	611.5	2.6	10.9
Aug	616.7	617.9	615.3	621.9	612.0	2.6	9.9
Sep	615.9	617.2	614.5	620.4	610.4	2.7	9.98
Oct	615.6	617.1	614.1	621.9	608.2	2.9	13.8
Nov	615.1	616.6	613.6	620.7	605.4	3.0	15.3
Dec	614.3	615.9	612.7	620.2	603.2	3.1	17.0
annual	615.1	616.5	613.6	621.2	606.2	2.95	15.1
std dev	1.6						
max	616.7	617.9	615.3	622.4	612.0	3.4	22.3
min	613.3	614.9	611.7	620.1	598.0	2.6	9.9

		UKIRT					
Jan	613.3	614.6	612.0	619.98	603.03	2.5	16.95
Feb	613.3	614.6	612.0	620	600.6	2.6	19.4
Mar	613.2	614.5	611.97	619.5	600.2	2.6	19.3
Apr	614.5	615.6	613.3	619.4	605.97	2.3	13.4
May	615.3	616.4	614.2	620.3	608.8	2.2	11.6
Jun	616.1	617.1	615.1	620.4	611.5	1.96	8.9
Jul	616.3	617.2	615.3	620.0	611.98	1.9	8.1
Aug	616.3	617.2	615.3	619.8	612.3	1.9	7.4
Sep	615.9	616.97	614.9	619.6	612.0	2.1	7.6
Oct	615.6	616.7	614.5	619.7	609.9	2.2	9.8
Nov	614.98	616.1	613.9	619.99	607.0	2.3	12.98
Dec	614.3	615.6	613.1	620.1	604.7	2.5	15.4
annual	614.9	616.1	613.1	619.9	607.3	2.97	12.6
std dev	1.1						
max	616.3	617.2	615.3	620.4	612.3	2.6	19.4
min	613.2	614.5	611.97	619.4	600.2	1.9	7.4

Table 3 : Temperature Analysis Results

			CFHT				
		temperature	C degrees				
	temp ave	mean of max (A)	mean of min (B)	abs max (AA)	abs min (BB)	A - B	AA - BB
Jan	0.3	3.6	-2.7	11.2	-10.9	6.4	22.1
Feb	-0.3	3.5	-3.5	10.9	-10.1	7.0	21.0
Mar	-0.2	3.4	-3.2	10.5	-9.8	6.6	20.3
Apr	1.4	5.3	-1.4	11.6	-7.3	6.7	18.9
May	2.4	6.2	-0.5	14.6	-5.7	6.7	20.3
Jun	4.0	7.8	1.1	15.0	-5.3	6.7	20.2
Jul	3.8	7.6	0.7	15.0	-4.9	6.9	19.9
Aug	3.9	7.8	1.1	15.0	-4.9	6.6	19.9
Sep	4.5	8.3	1.6	11.9	-2.9	6.6	14.8
Oct	3.2	6.7	0.4	10.5	-5.4	6.3	15.9
Nov	1.9	5.1	-0.7	11.4	-7.2	5.8	18.6
Dec	1.3	4.5	-1.4	10.4	-10.2	5.9	20.5
annual	2.2	5.8	-0.7	12.3	-7.1	6.5	19.4
std dev	1.6						
max	4.5	8.3	1.6	15.0	-2.9	6.9	22.1
min	-0.3	3.4	-3.5	10.4	-10.9	5.8	14.8

		UKIRT					
Jan	0.1	3.3	-2.9	11.7	-13.8	6.2	25.5
Feb	-0.2	3.5	-3.3	12.6	-11.6	6.8	24.2
Mar	0.1	4.3	-3.4	12.7	-10.3	7.7	23.0
Apr	1.9	6.5	-2.2	14.7	-8.5	8.7	23.2
May	2.7	7.8	-1.1	16.3	-7.1	8.9	23.3
Jun	4.4	9.9	0.3	16.7	-7.9	9.6	24.5
Jul	4.1	9.3	0.1	16.5	-6.1	9.3	22.6
Aug	4.1	9.9	0.7	16.8	-4.1	9.2	20.9
Sep	4.4	9.8	1.0	16.3	-4.3	8.8	20.6
Oct	3.2	7.8	-0.2	14.2	-7.0	8.0	21.2
Nov	1.9	5.8	-1.1	11.8	-7.6	6.9	19.4
Dec	1.2	4.3	-1.96	12.3	-10.6	6.2	22.9
annual	2.3	6.9	-1.2	14.4	-8.2	8.0	22.6
std dev	1.7						
max	4.4	9.9	1.0	16.8	-4.1	9.6	25.5
min	-0.2	3.3	-3.4	11.7	-13.8	6.2	19.4

Table 4 Wind speed Analysis Results

		CFHT	wind speed	in m/s			
	ave	ave of max (A)	ave of min (B)	abs max (AA)	abs min (BB)	A - B	AA - BB
Jan	10.2	16.2	3.7	41.1	0.5	12.5	40.6
Feb	7.9	14.3	2.7	40.8	0.1	11.6	40.7
Mar	8.5	14.3	2.7	31.1	1.8	11.6	29.3
Apr	5.8	11.1	1.6	26.6	0.1	9.5	26.5
May	6.8	12.2	2.2	30.6	0.1	10.0	30.6
Jun	5.7	10.8	1.4	25.7	0.04	9.4	25.6
Jul	6.1	11.6	1.7	25.6	0.07	9.9	25.5
Aug	5.6	11.1	1.3	25.6	0.07	9.7	25.6
Sep	4.7	9.6	0.9	20.3	0.07	8.7	20.3
Oct	6.2	11.2	1.6	25.5	0.04	9.6	25.4
Nov	6.3	11.6	1.7	30.7	0.07	9.9	30.6
Dec	8.1	14.3	2.6	40.7	0.07	11.6	40.6
annual	6.8	12.4	2.0	30.6	0.25	10.4	30.2
std dev	1.5						
max	10.2	16.2	3.7	41.1	1.8	12.5	40.7
min	4.7	9.6	0.9	20.4	0.04	8.7	20.3

		UKIRT					
	ave	ave of max (A)	ave of min (B)	abs max (AA)	abs min (BB)	A - B	AA - BB
Jan	7.0	10.9	3.6	42.1	0.1	7.2	42.0
Feb	5.4	9.1	2.2	34.1	0.1	6.9	34.0
Mar	5.1	9.2	2.3	34.9	0.1	6.9	34.8
Apr	3.4	6.4	1.1	28.4	0.1	5.3	28.3
May	3.5	6.2	1.2	16.7	0.004	4.9	16.7
Jun	2.6	4.7	0.6	18.3	0.015	4.1	18.3
Jul	2.8	5.0	0.7	13.8	0.014	4.3	13.8
Aug	2.4	4.6	0.4	17.9	0.01	4.2	17.9
Sep	2.4	4.6	0.4	14.2	0.014	4.3	14.2
Oct	3.0	5.6	0.8	10.6	0.005	4.8	10.6
Nov	3.4	6.2	1.1	10.9	0.006	5.2	10.9
Dec	4.5	7.6	1.6	20.4	0.01	6.0	20.4
annual	3.8	6.7	1.3	21.9	0.04	5.3	21.8
std dev	1.4						
max	7.0	10.9	3.6	42.1	0.1	7.2	42.0
min	2.4	4.6	0.4	10.6	0.01	4.1	10.6

Table 5 Results of Analysis for El Niño (1997-1998) and La Niña (1998 – 1999) years.

	CFHT				
	normal	El Niño		La Niña	
	pressure	hPa			
			dp		dp
Dec	614.3	614.6	0.4	614.7	0.4
Jan	613.5	614.8	1.3	613.0	-0.5
Feb	613.3	616.7	3.4	613.9	0.6
Mar	613.4	615.1	1.7	613.3	-0.1
mean	613.6	615.3		613.7	
dmean			1.7		0.1
	temp	Celsius			
			dT		dT
Dec	1.5	2.0	0.5	0.9	-0.6
Jan	0.3	3.8	2.3	-1.3	-1.6
Feb	-0.3	3.6	2.2	-1.4	-1.1
Mar	-0.1	1.7	0.2	-0.7	-0.6
mean	0.3	2.8		-0.7	
dmean			2.5		-1.0
	wind	speed	m/s		
			dws		dws
Dec	8.1	6.2	-1.8	7.8	-0.3
Jan	10.2	7.4	-0.7	11.1	0.9
Feb	7.9	5.3	-2.8	10.2	2.2
Mar	8.5	7.4	-0.7	6.9	-1.7
mean	8.6	6.6		9.0	
dmean			-2.0		0.4
	relative	humidity	%		
			dRH		dRH
Dec	33.0	13.9	-19.2	33.2	0.2
Jan	38.6	24.3	-8.7	38.9	0.3
Feb	38.6	19.1	-13.9	35.1	-3.5
Mar	37.7	16.2	-16.8	25.7	-11.9
mean	37.0	18.4		33.2	
dmean			-18.6		-3.7

Table 5 Results of analysis for El Niño (1997-1998) and La Niña (1998 – 1999) years.

	UKIRT				
	normal	El Niño		La Niña	
	pressure	hPa			
			dp		dp
Dec	614.3	614.8	0.6	614.9	0.6
Jan	613.3	615.0	0.7	613.4	-0.9
Feb	613.2	616.7	2.4	614.2	-0.03
Mar	613.2	615.5	1.3	613.7	-0.5
mean	613.5	615.5		614.0	
dmean			2.0		0.6
	temperature	Celsius	degrees		
			dT		dT
Dec	1.2	0.6	-0.6	1.1	-0.1
Jan	0.1	2.5	1.4	-1.1	-2.3
Feb	-0.2	3.2	2.1	-1.0	-2.2
Mar	0.1	3.1	1.9	-0.6	-1.8
mean	0.3	2.4		-0.4	
dmean			2.1		-0.7
	wind speed	m/s			
			dws		dws
Dec	4.8	2.9	-1.9	2.0	-2.8
Jan	7.6	4.6	-0.2	3.1	-1.7
Feb	5.9	3.0	-1.8	1.8	-3.0
Mar	5.5	3.0	-1.8	1.5	-3.3
mean	5.9	3.4		2.1	
dmean			-2.6		-3.9
	relative	humidity	%		
			dRH		dRH
Dec	31.6	14.7	-16.9	13.8	-17.7
Jan	35.7	11.8	-19.7	48.6	17.1
Feb	35.6	12.5	-19.0	36.2	4.7
Mar	35.2	13.6	-18.0	33.8	2.2
mean	34.5	13.2		33.1	
dmean			-21.4		-1.4

Table 5 continued, Results of analysis for El Niño (1997-1998) and La Niña (1998 – 1999) years.

	UKIRT				
	normal	El Niño		La Niña	
	dew	point	C		
			dTd		dTd
Dec	-18.56	-26.2	-7.7	-17.3	1.3
Jan	-17.742	-25.3	-6.7	-14.8	3.7
Feb	-17.886	-24.0	-5.4	-19.1	-0.5
Mar	-17.337	-22.3	-3.8	-18.2	0.3
mean	-17.88125	-24.5		-17.4	
dmean			-6.6		0.5
	mixing	ratio	g/Kg		
			dw		dw
Dec	2.0	0.8	-1.2	2.2	0.2
Jan	2.1	0.9	-1.1	2.6	0.6
Feb	2.0	1.1	-1.0	1.9	-0.1
Mar	2.1	1.2	-0.8	1.9	-0.2
mean	2.1	1.0		2.2	
dmean			-1.1		0.1

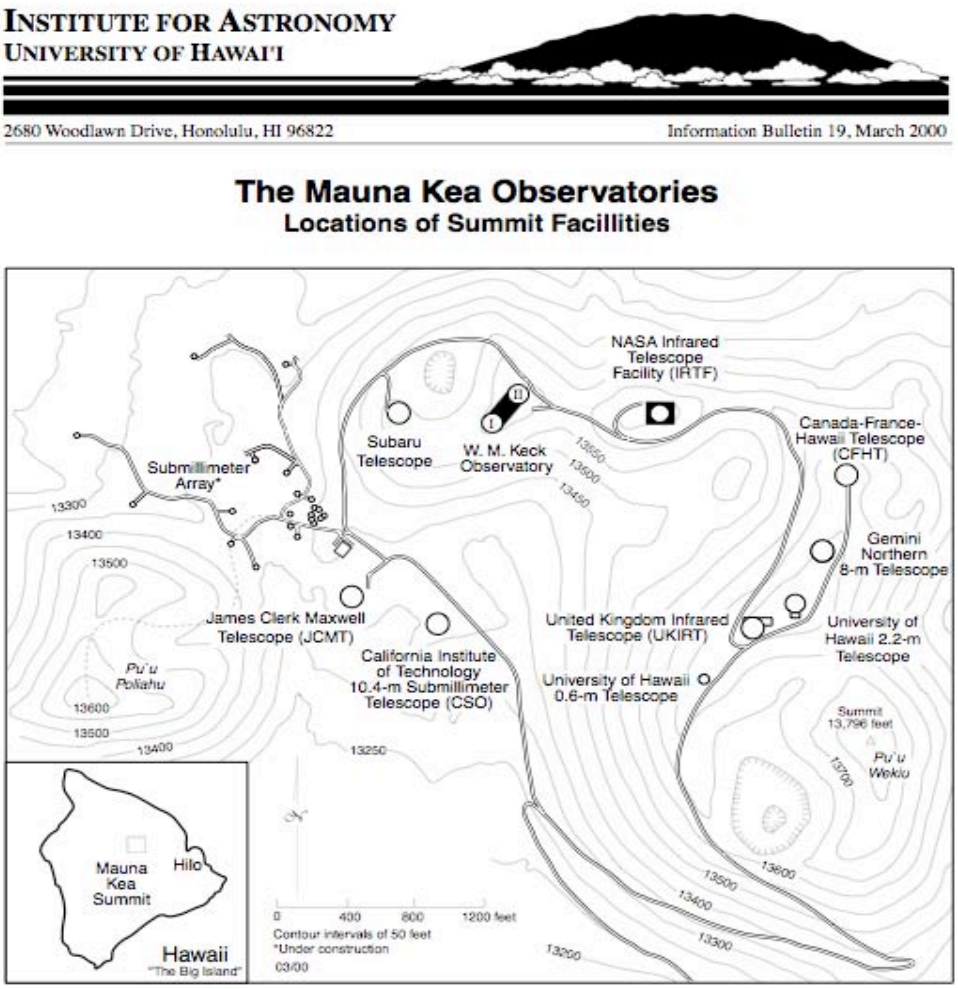

Fig. 1: Map of Mauna Kea Summit

Fig. 2: Photograph of the Summit of Mauna Kea, observatories

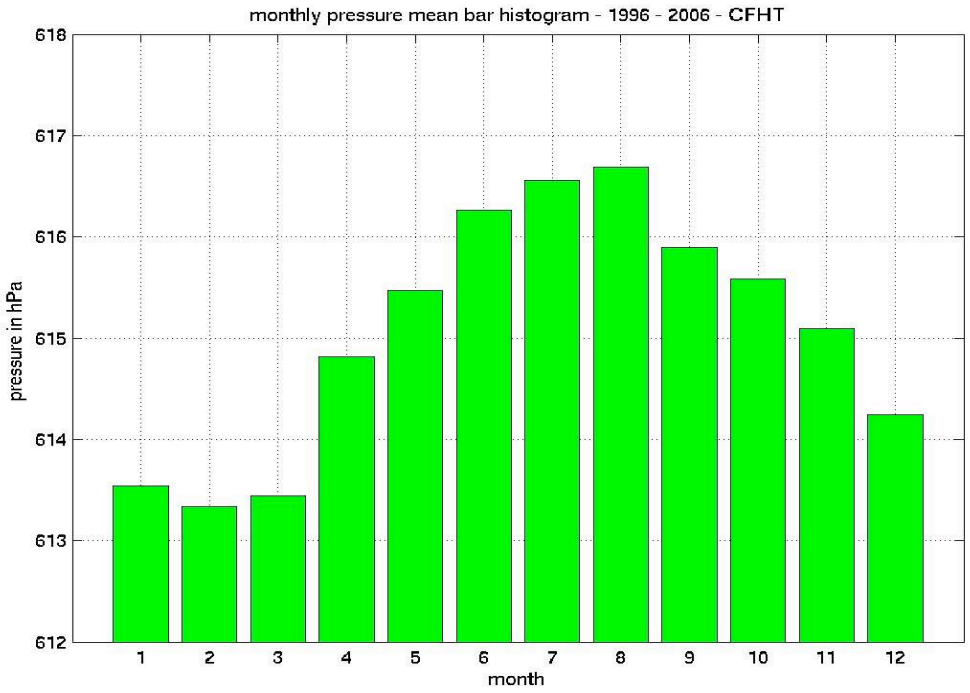

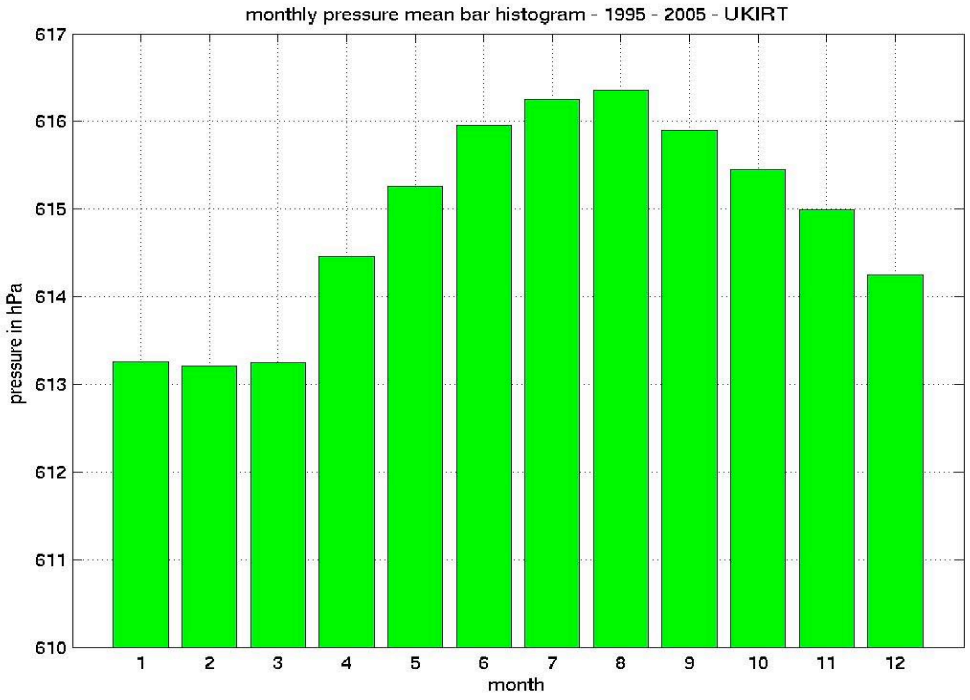

Fig. 3: Monthly mean bar plot for pressure, CFHT and UKIRT

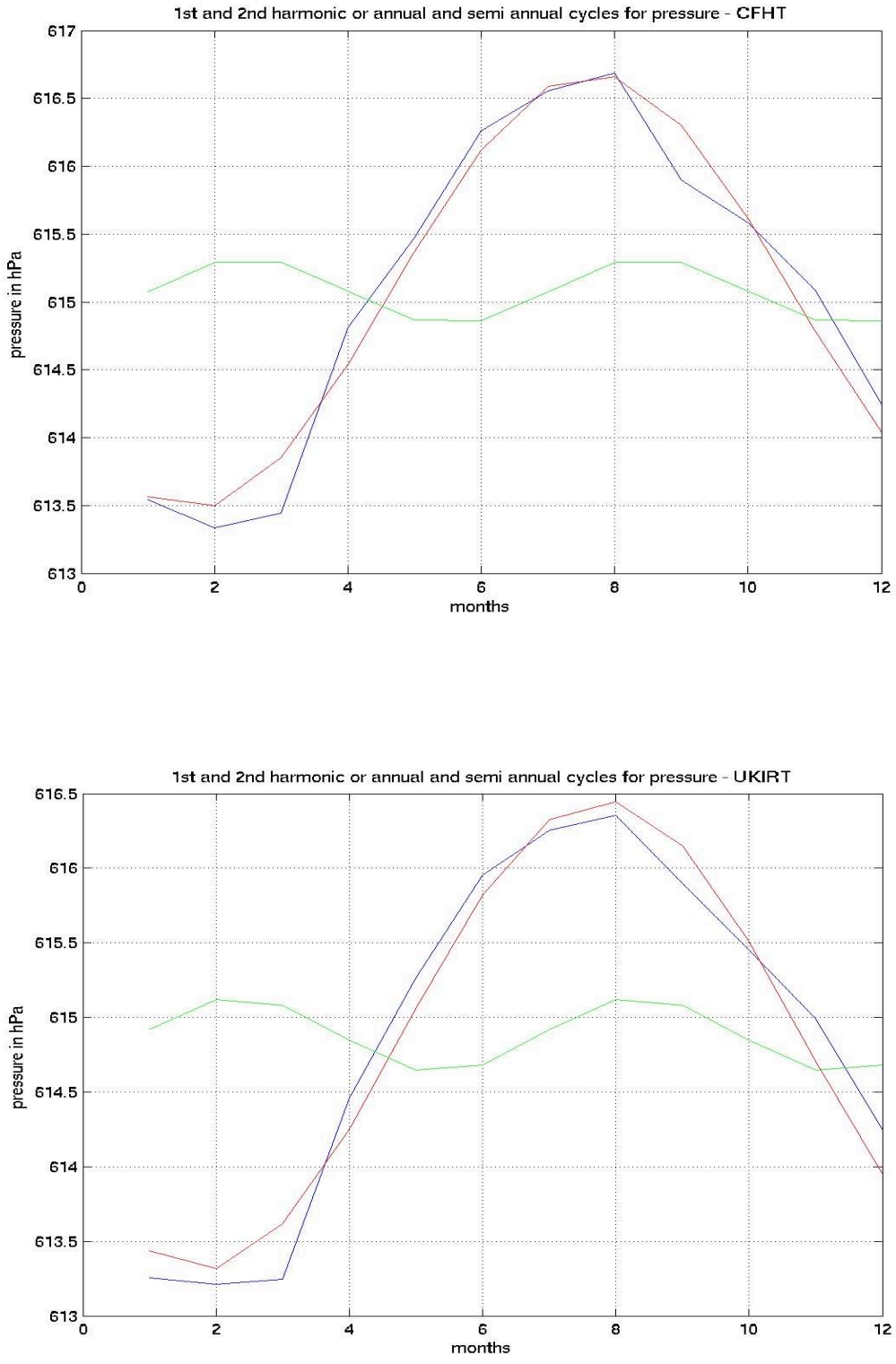

Fig. 4: Pressure annual cycle and monthly mean plot. Blue line: monthly mean curve; red line: 1st harmonic: annual cycle; green line: 2nd harmonic : semi annual cycle.

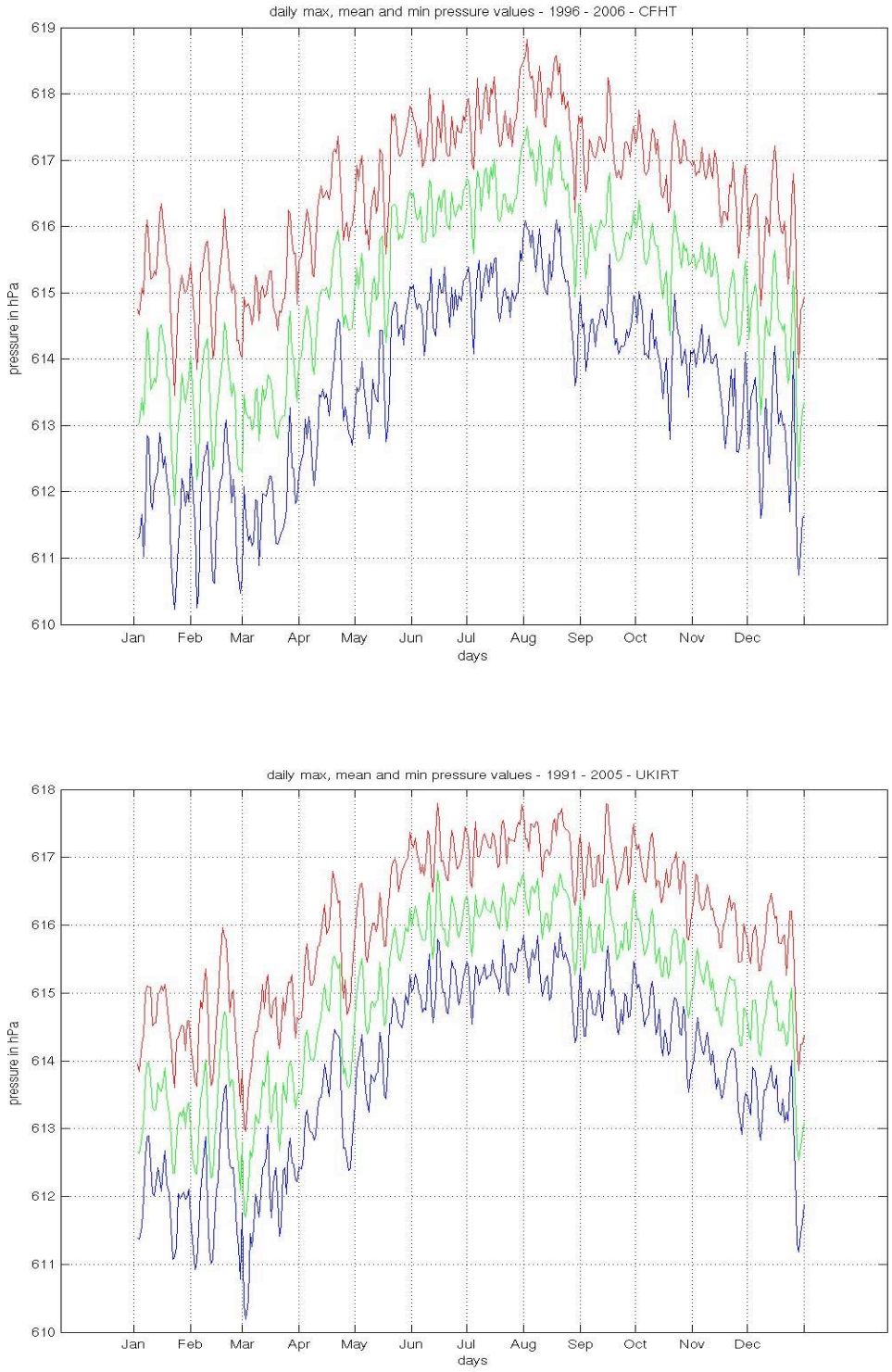

Fig. 5: Daily mean, mean of maximum and mean of minimum of pressure. Green line: pressure mean along the year, red line: mean of maximum pressure values along the year; blue line: mean of minimum pressure values along the year.

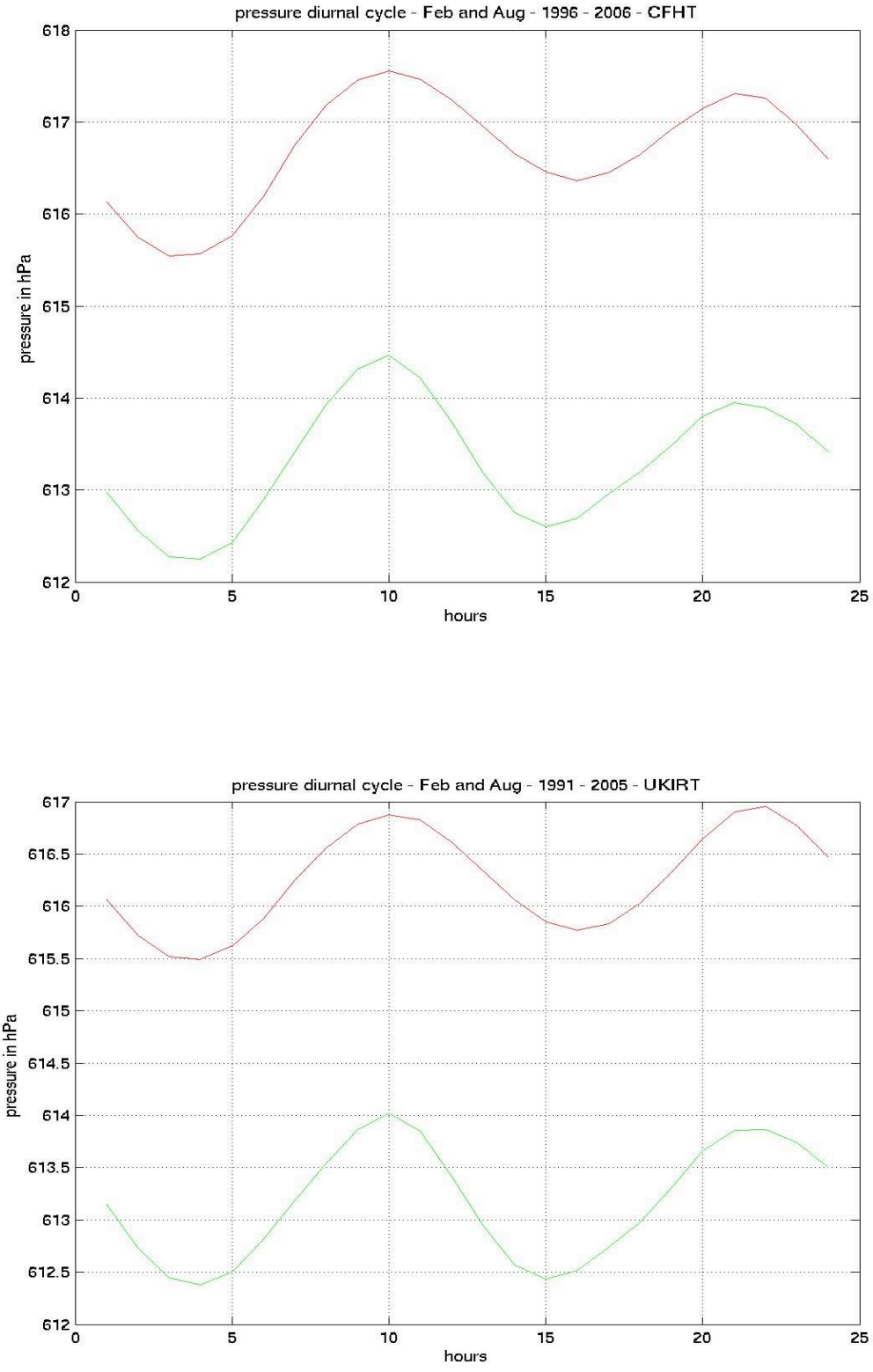

Fig. 6: Pressure semi diurnal cycle. Green line: February diurnal cycle; red line: August diurnal cycle

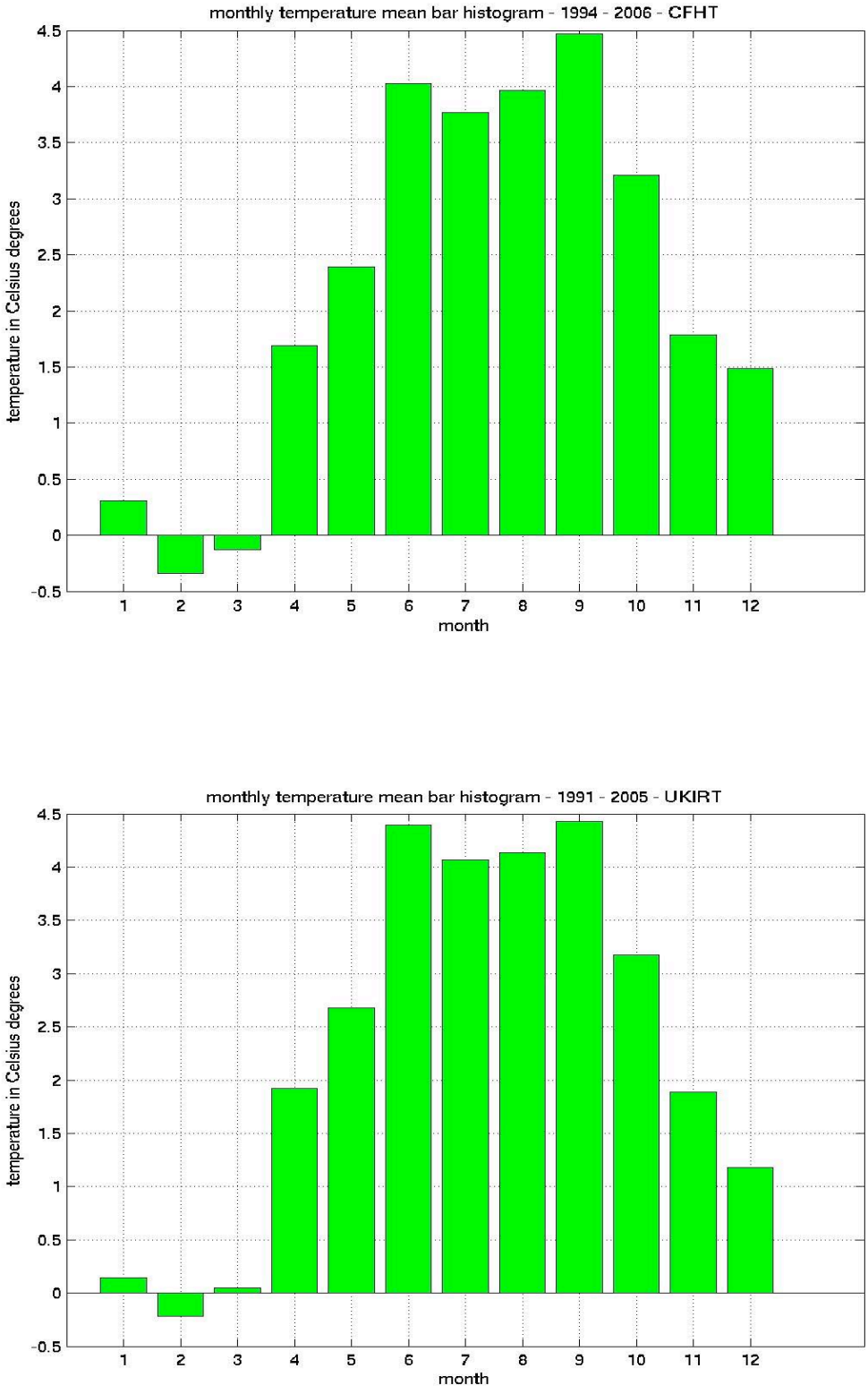

Fig. 7: Monthly mean bar plot for temperature, CFHT and UKIRT.

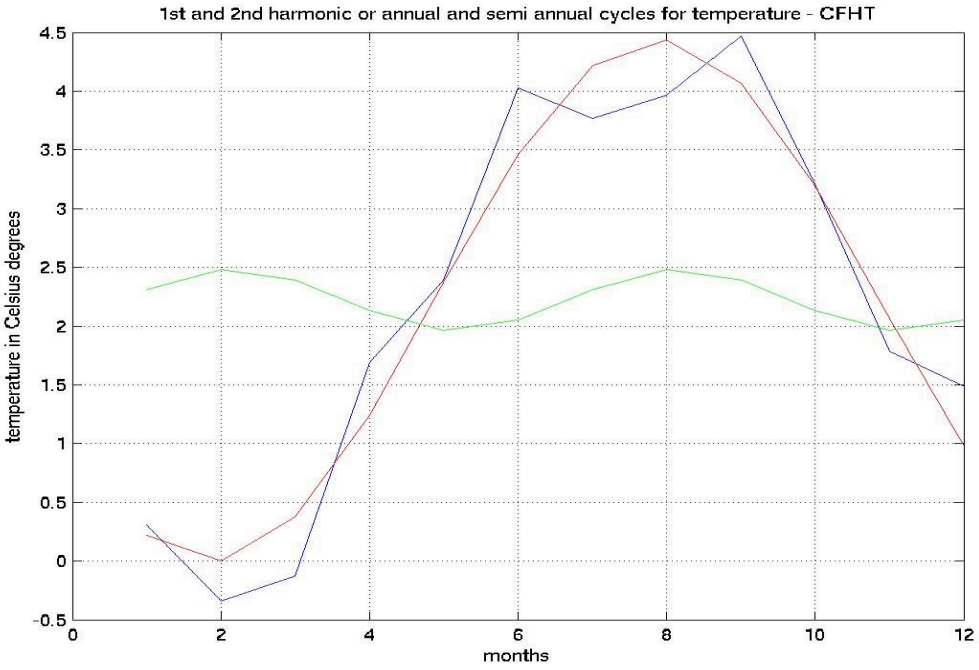

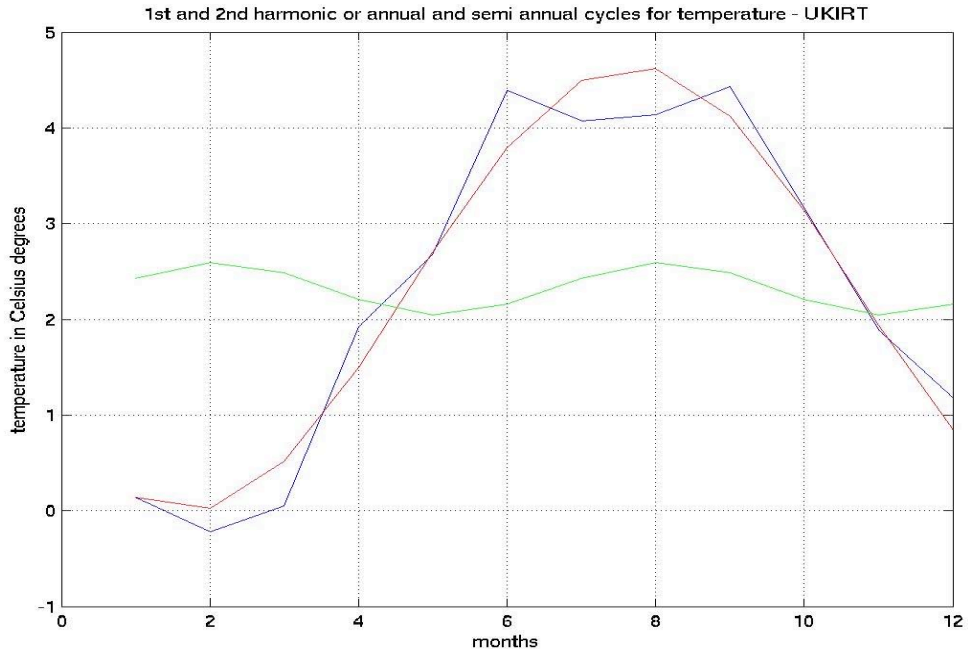

Fig. 8: Temperature annual cycle and monthly mean plot. Blue line: monthly mean curve; red line: 1st harmonic: annual cycle; green line: 2nd harmonic: semi – annual cycle.

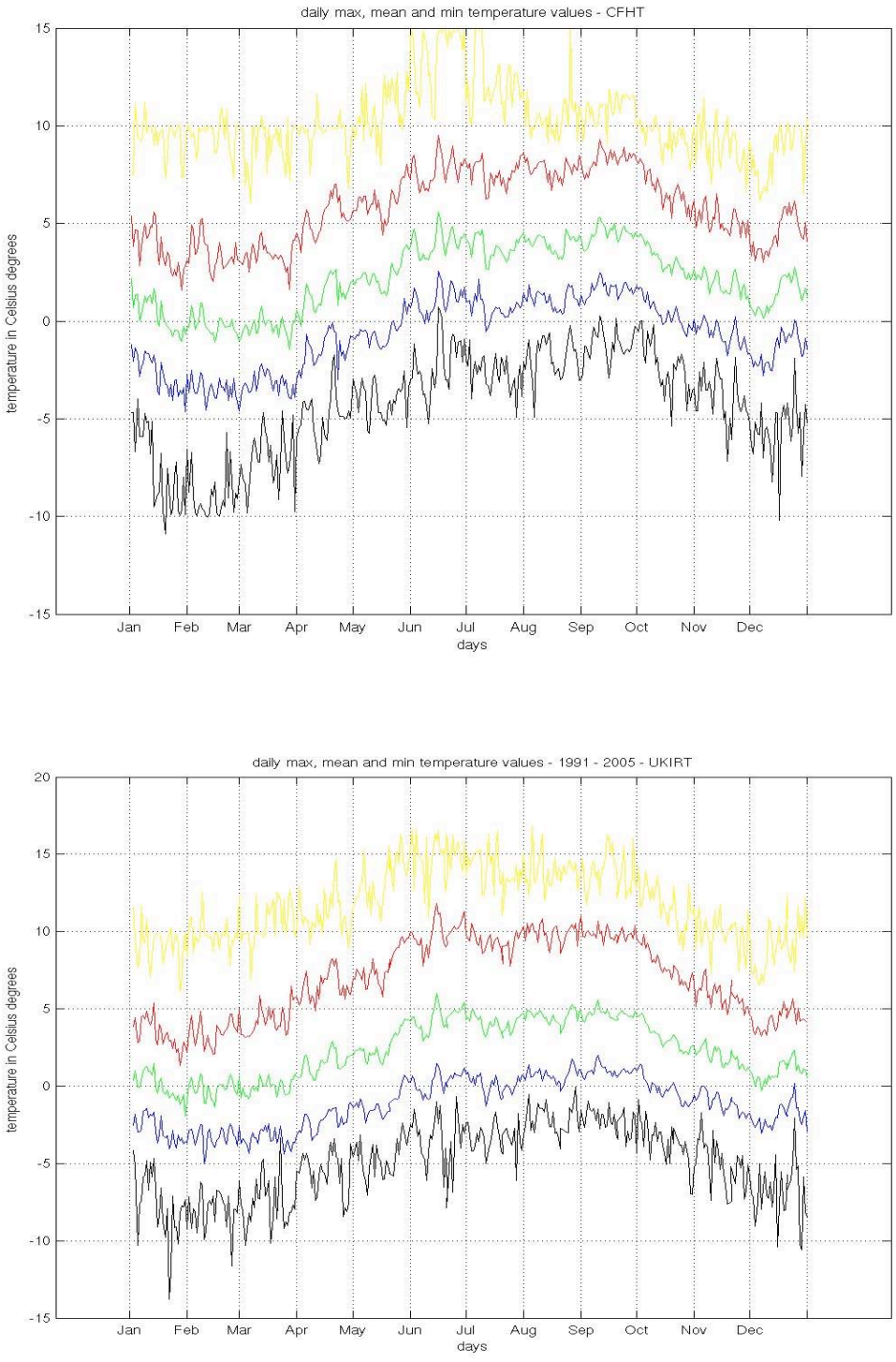

Fig. 9: Daily mean, mean of maximum and mean of minimum temperature. Green line: temperature mean along the year; red line: mean of maximum temperature along the year; blue line: mean of minimum temperature along the year; yellow line: absolute maximum temperature along the year; black line: absolute minimum temperature along the year.

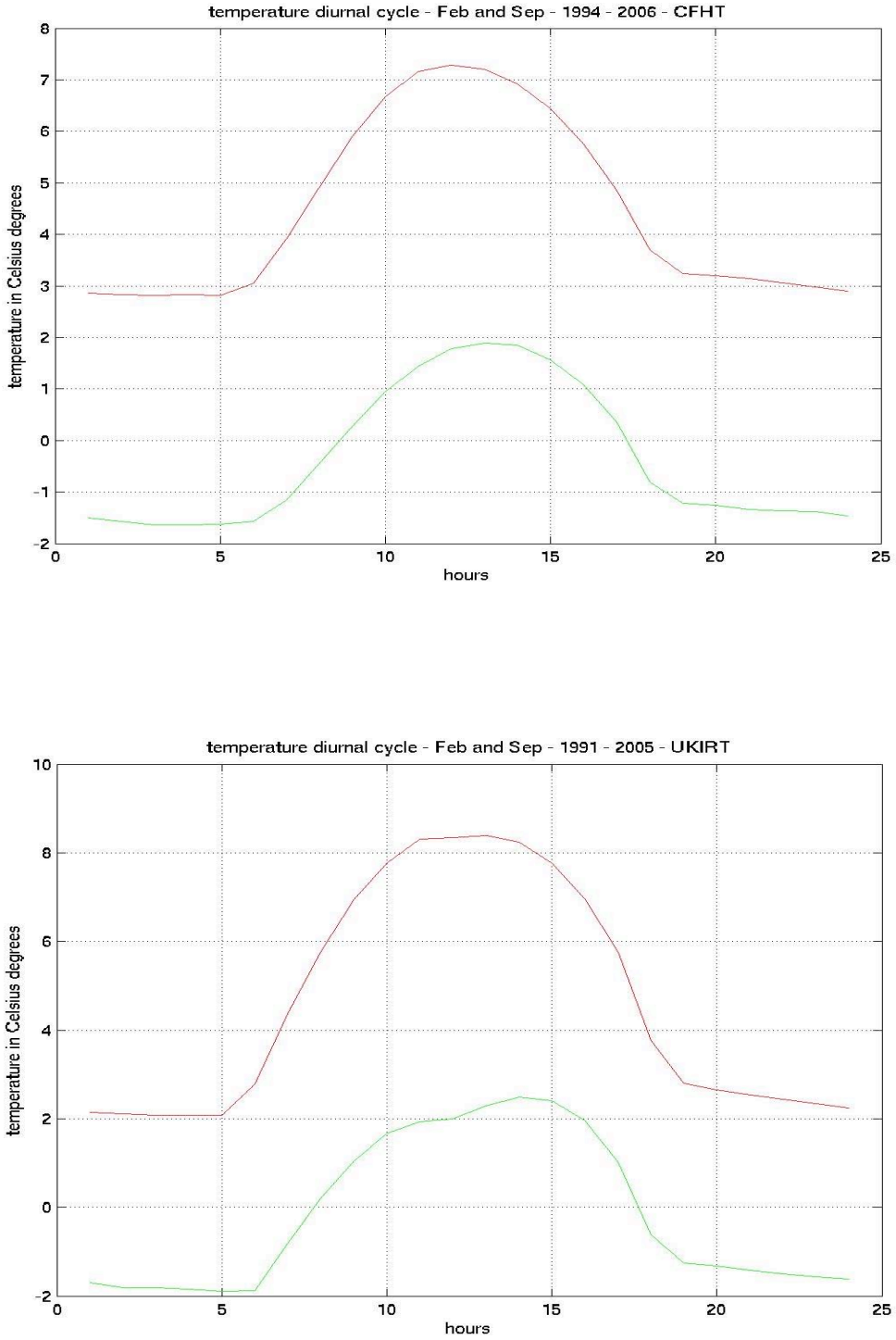

Fig. 10: Temperature diurnal cycle. Green line: February diurnal cycle; red line: September diurnal cycle.

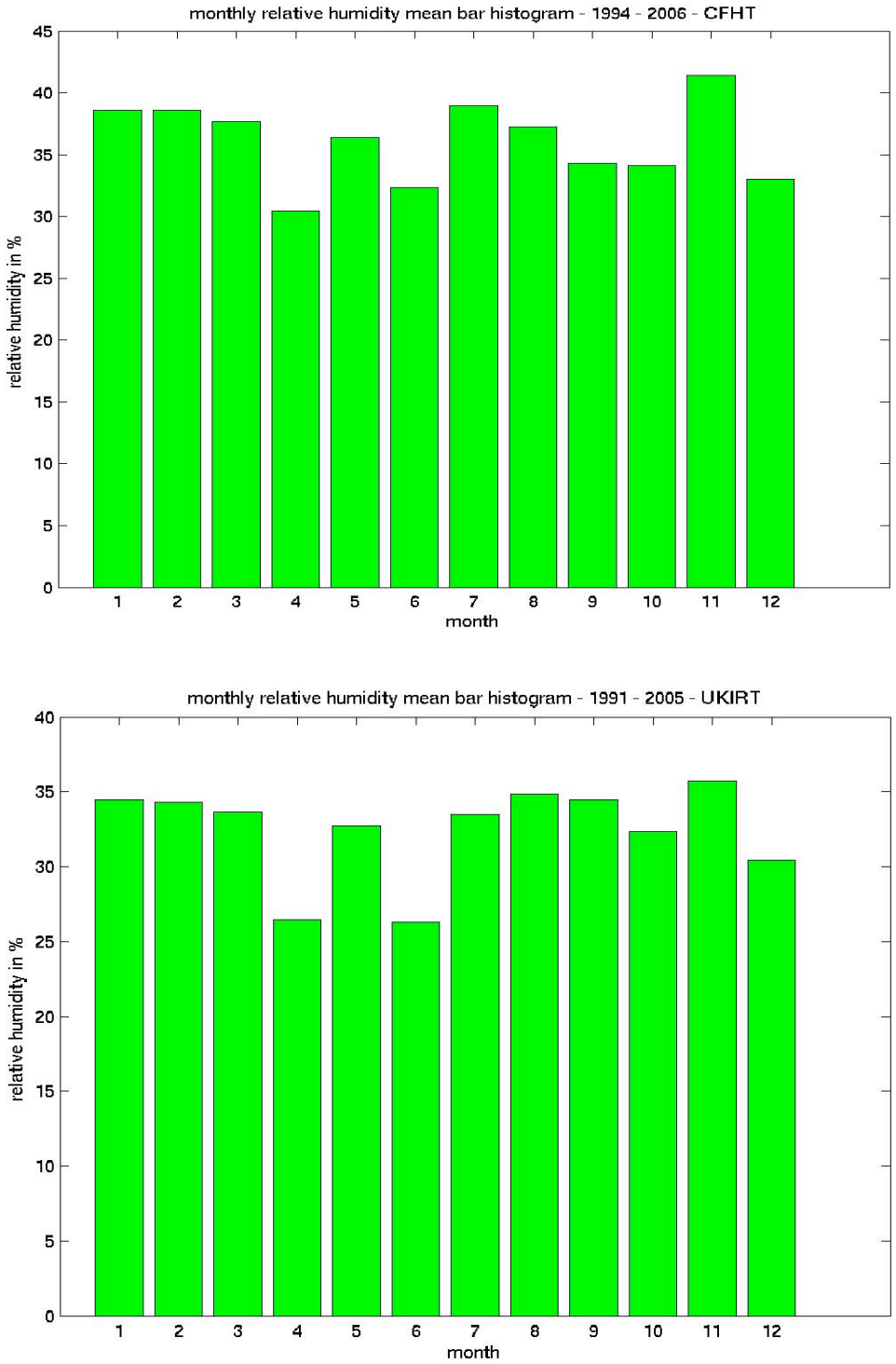

Fig. 11: Monthly mean bar for Relative Humidity.

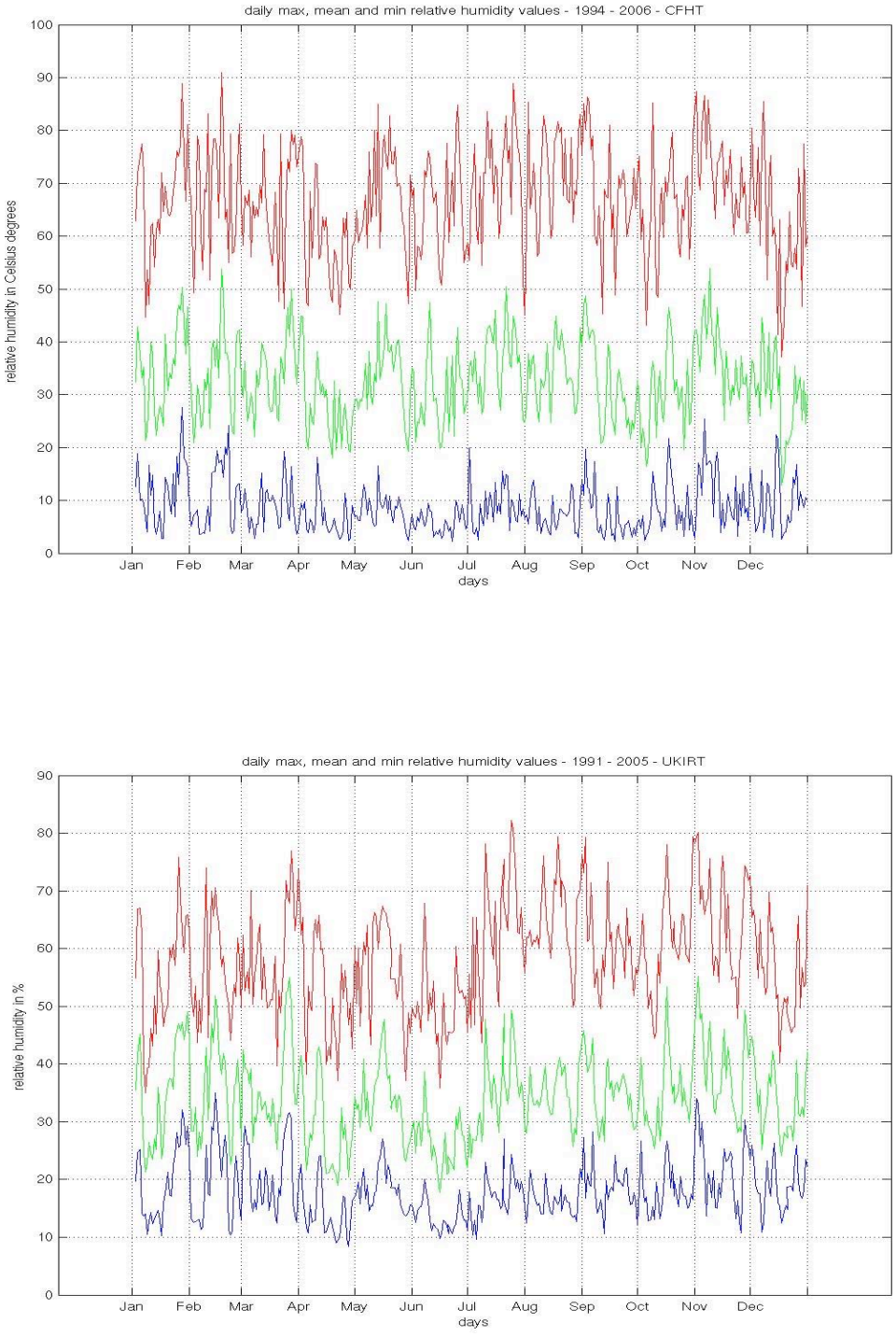

Fig. 12: Daily mean, mean of maximum and mean of minimum relative humidity. Green line: relative humidity mean along the year; red line: mean of maximum relative humidity along the year; blue line: mean of minimum relative humidity along the year.

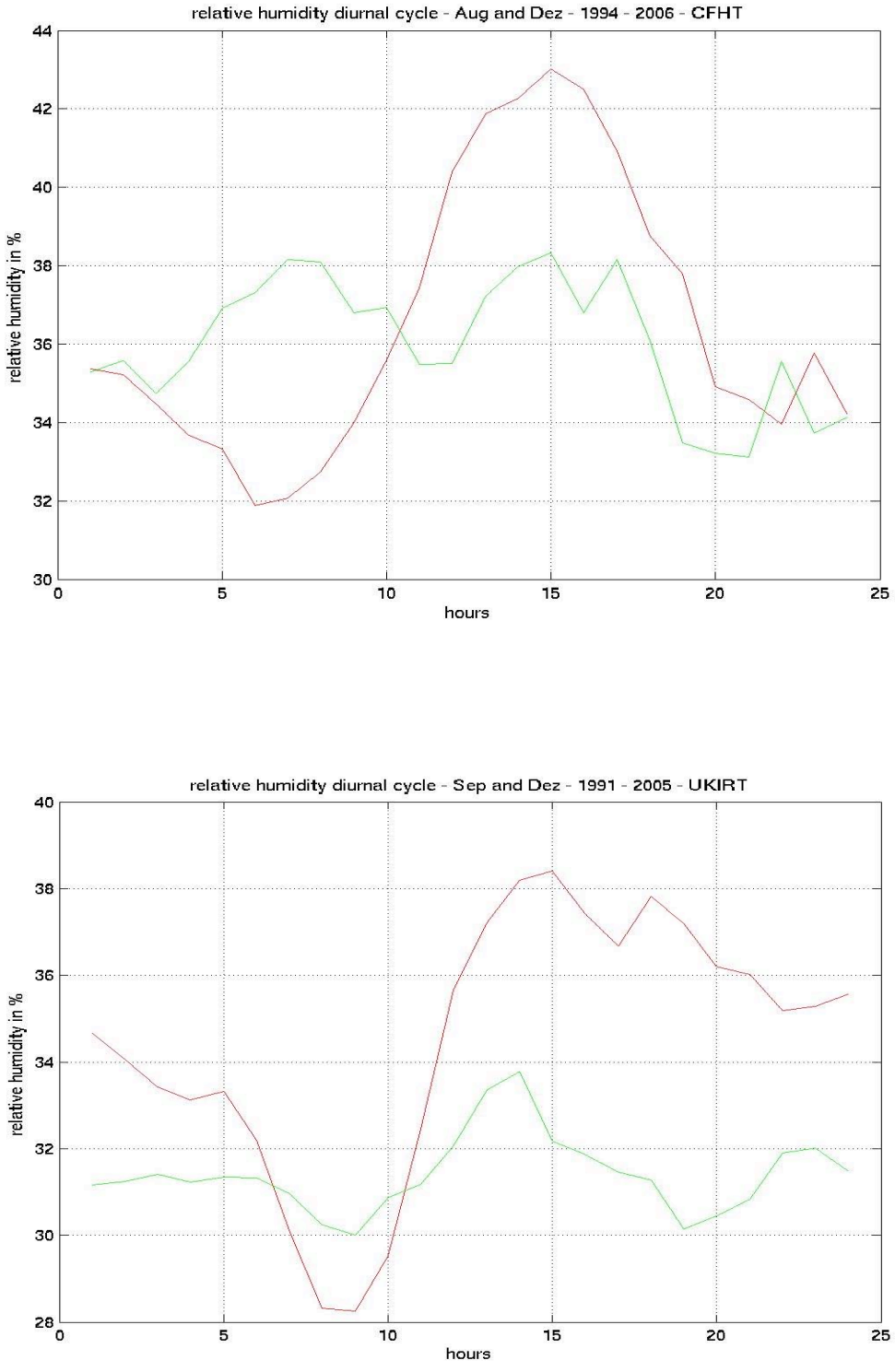

Fig. 13: Relative Humidity diurnal cycle. Red line: August – CFHT; September – UKIRT; green line: December.

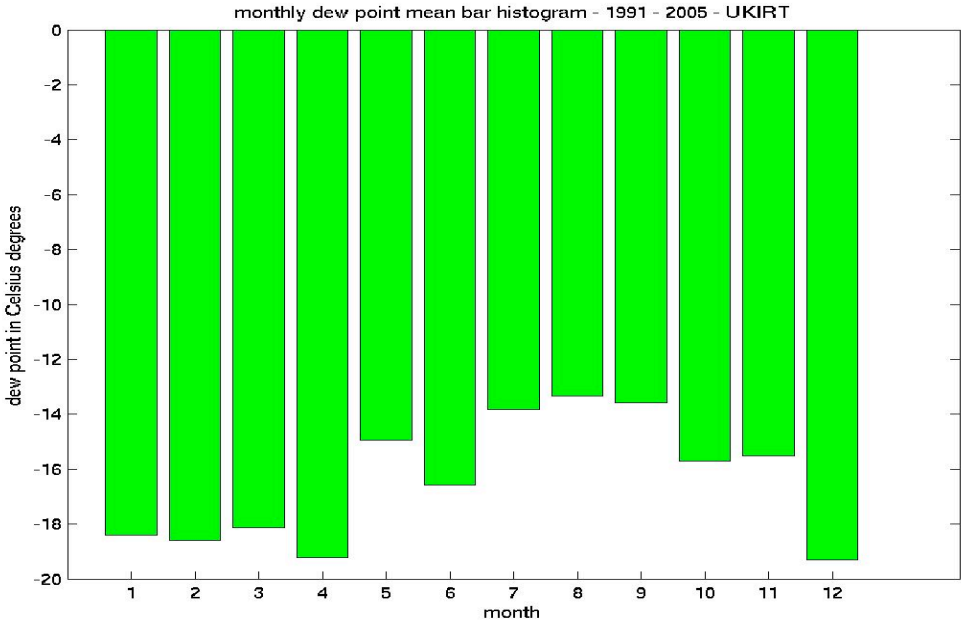

Fig. 14: Monthly mean bar plot for dew point – UKIRT

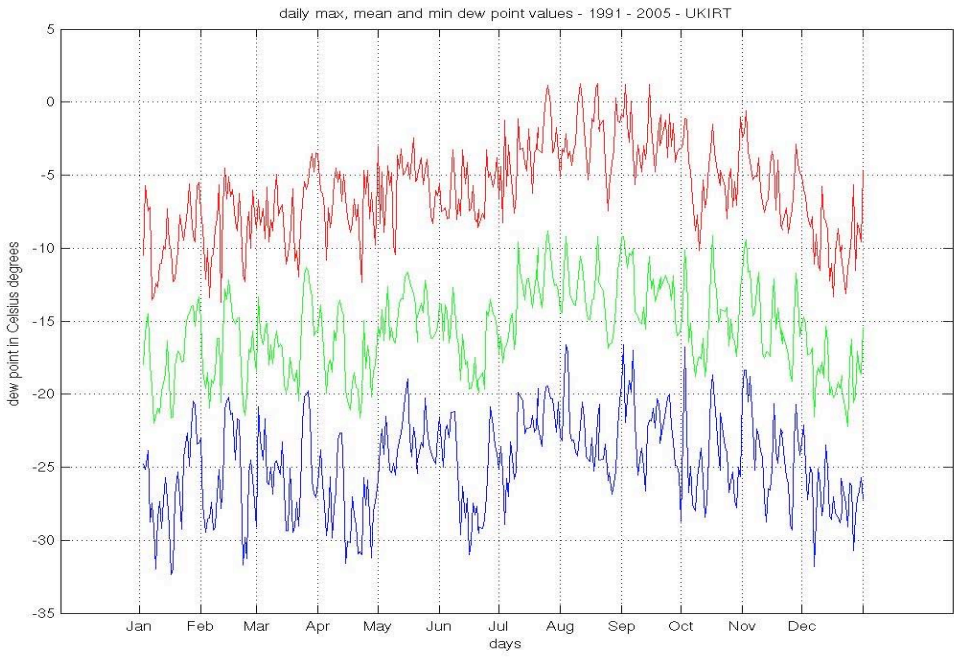

Fig. 15: Daily mean, mean of maximum and mean of minimum dew point. Green line: dew point mean along the year; red line: mean of maximum dew point along the year; blue line: mean of minimum dew point along the year.

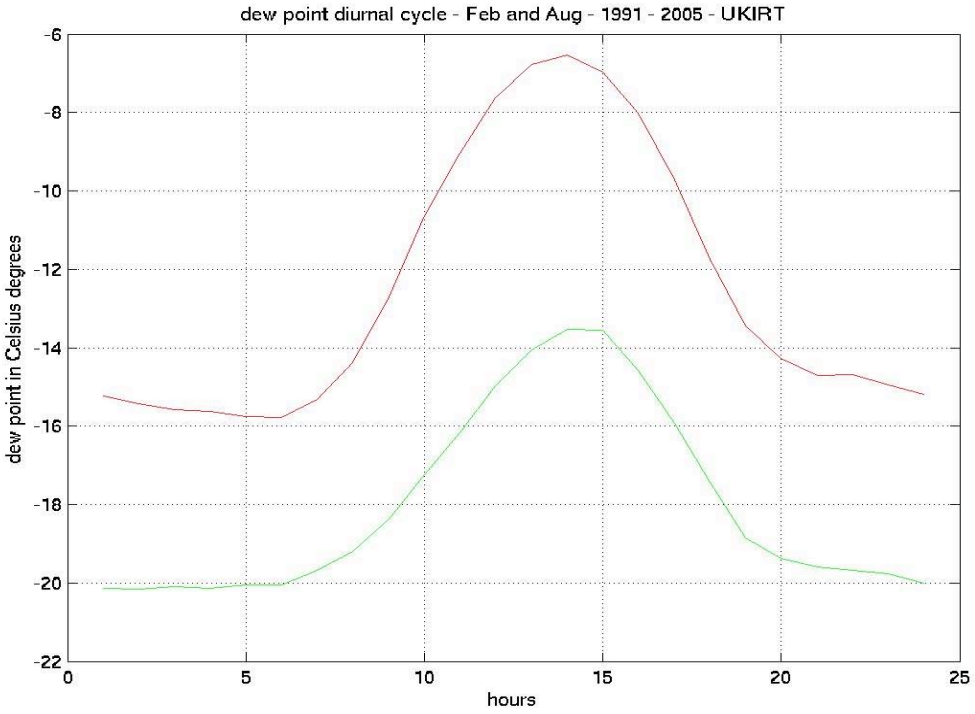

Fig 16: Dew point diurnal cycle. Green line: February; red line: August.

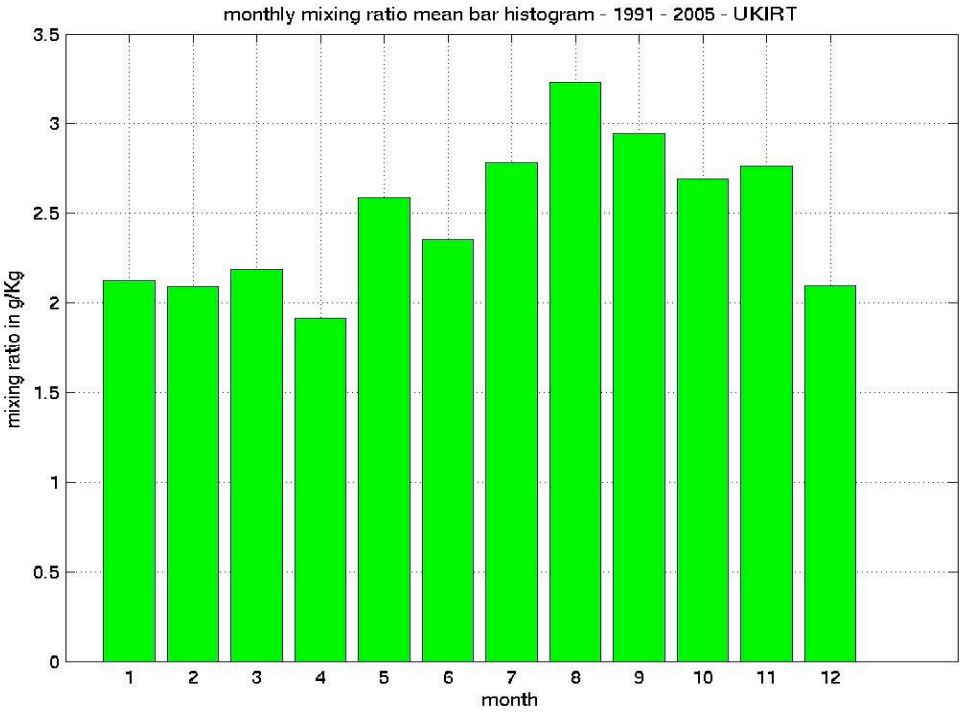

Fig. 17: Monthly mean bar plot for mixing ratio - UKIRT

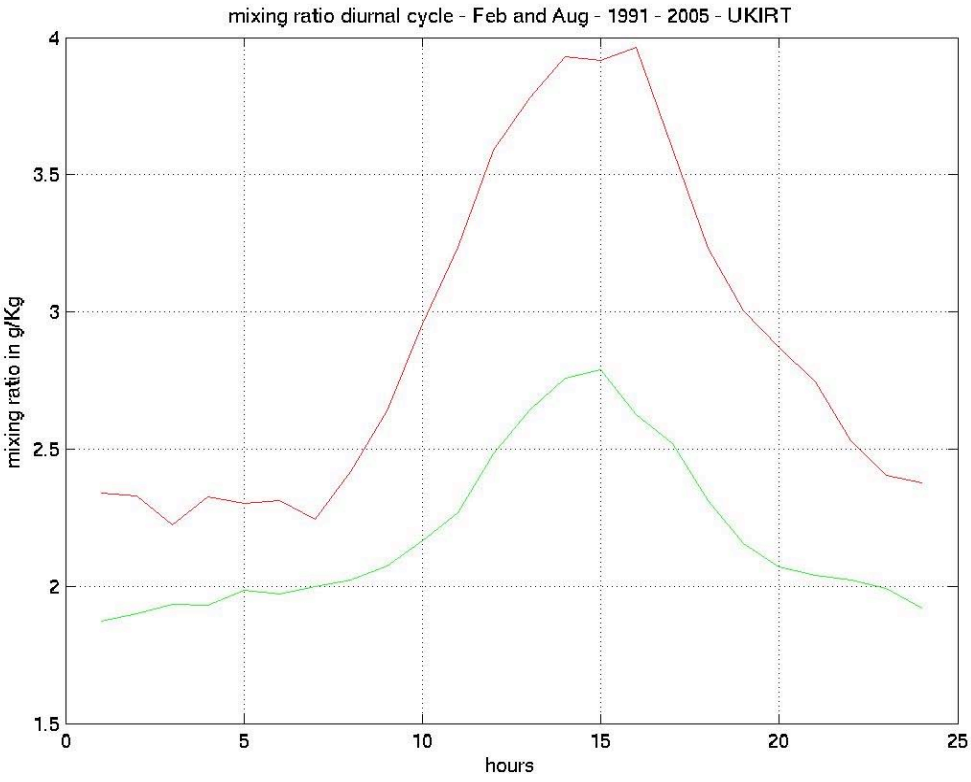

Fig. 18: Mixing ratio diurnal cycle. Green line: February; red line: August

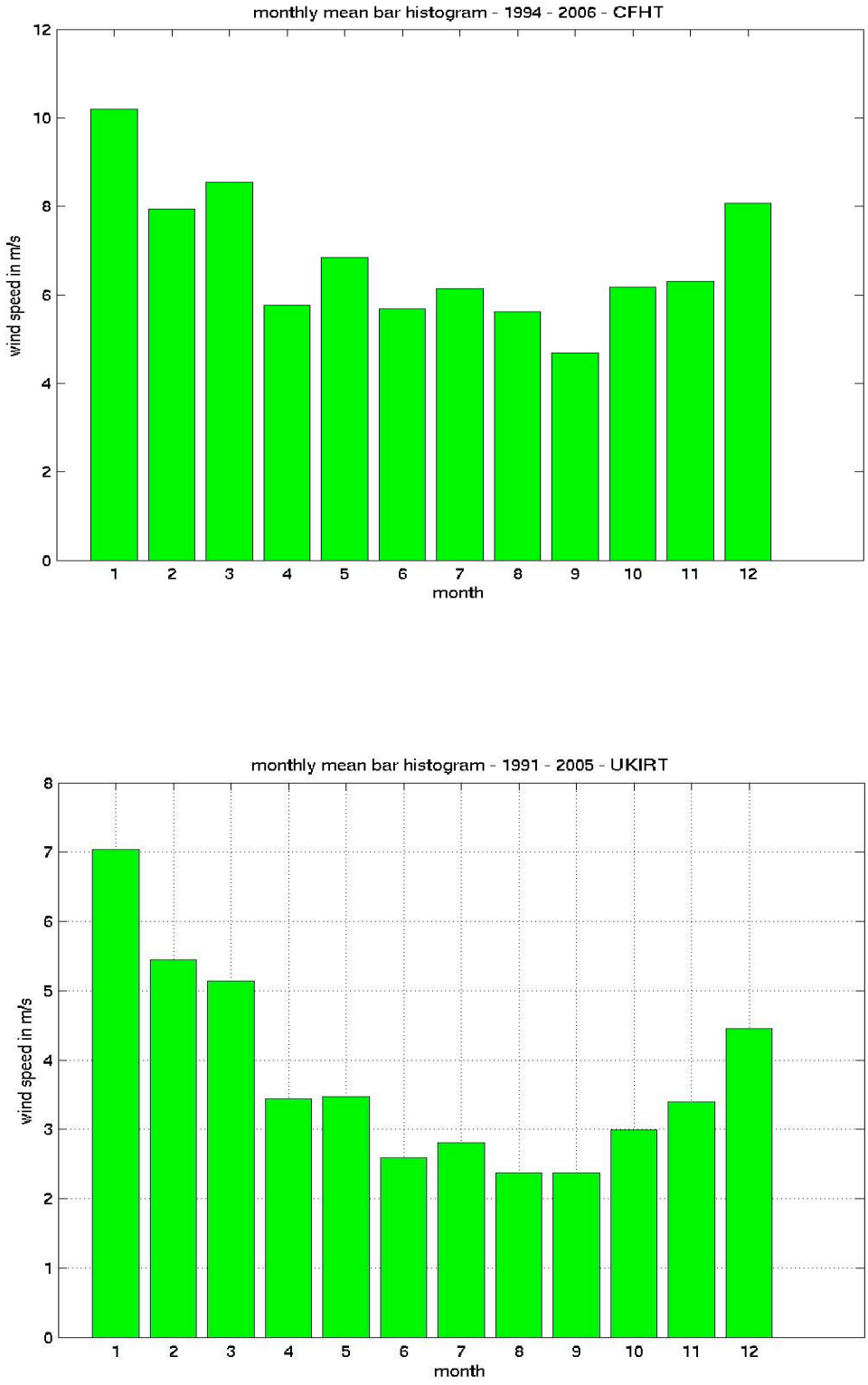

Fig. 19: Monthly mean bar plot for wind speed.

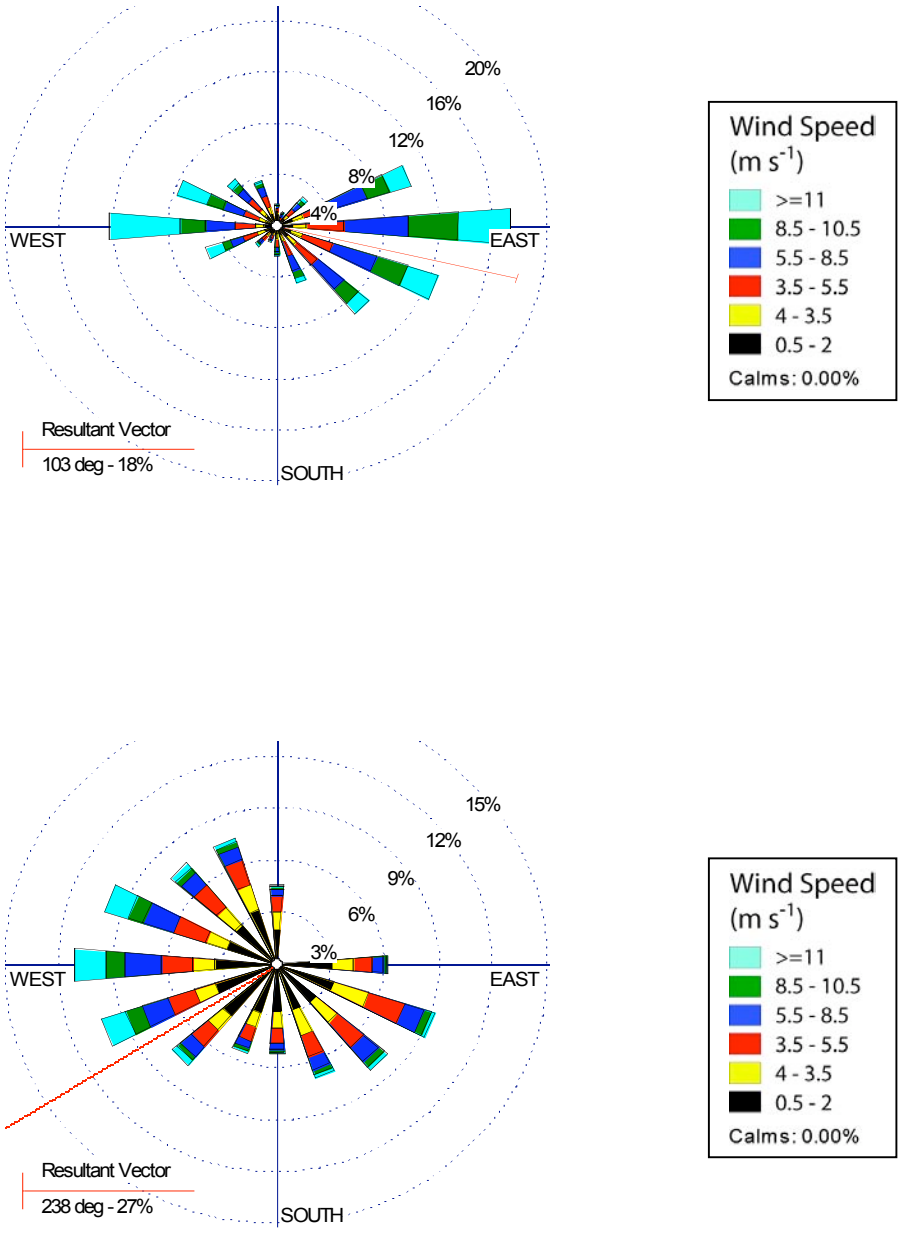

Fig. 20: Wind Rose plots for all months: up: 1994 – 2006 – CFHT; below: 1991 – 2005 – UKIRT

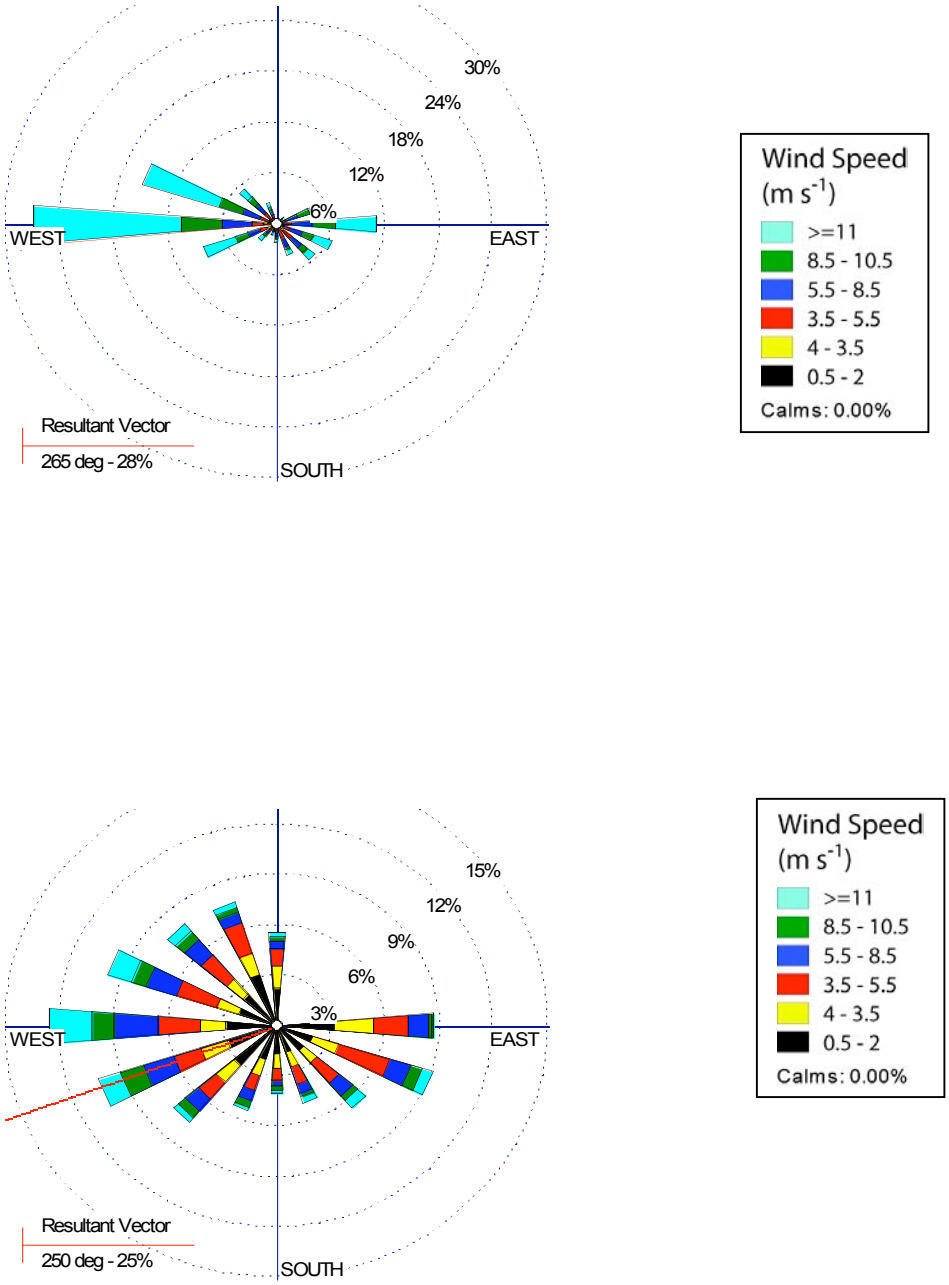

Fig. 21: Wind Rose for January; up: CFHT, bellow: UKIRT

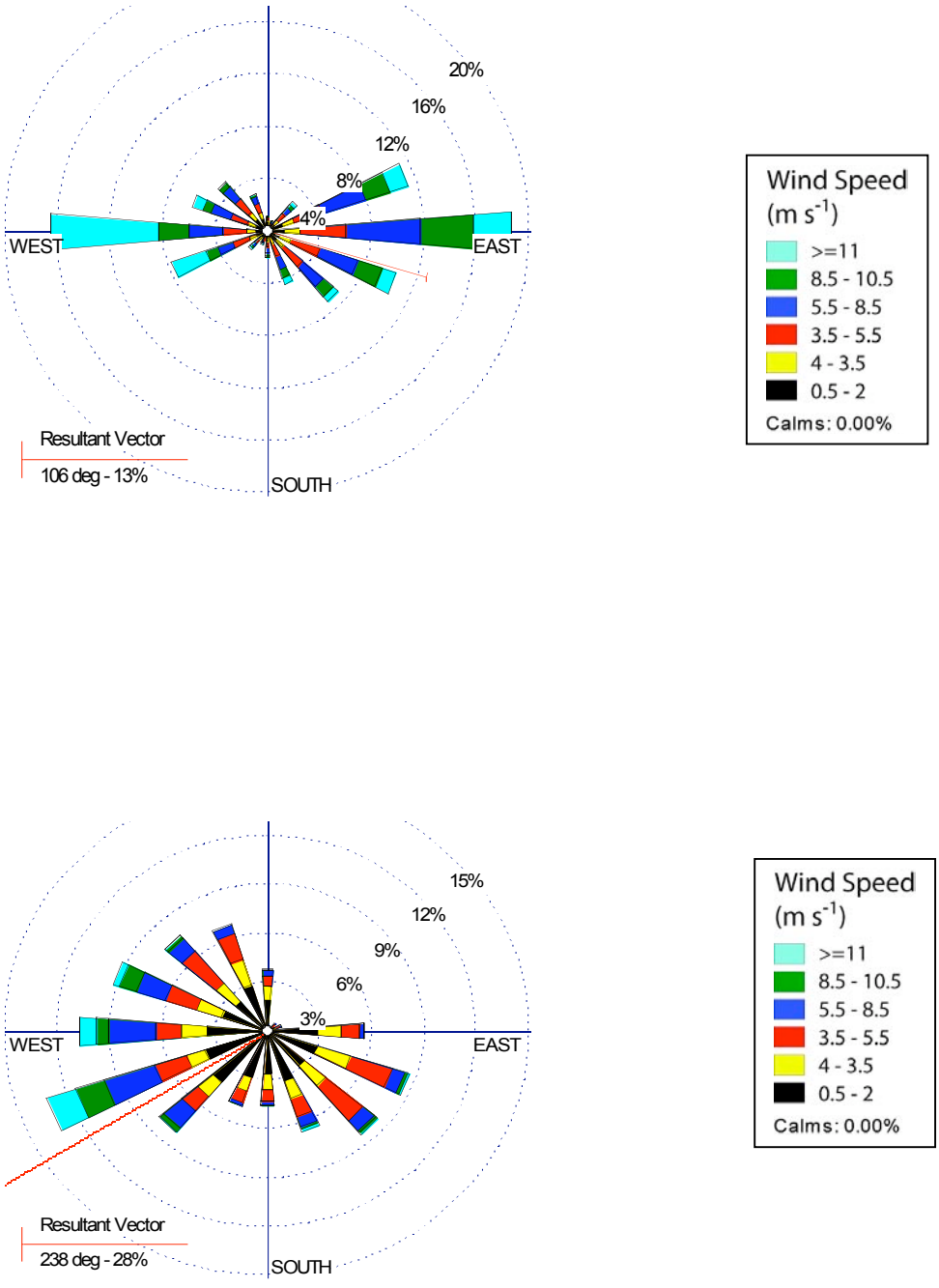

Fig. 22: Wind Rose plots for May; up: CFHT, below: UKIRT

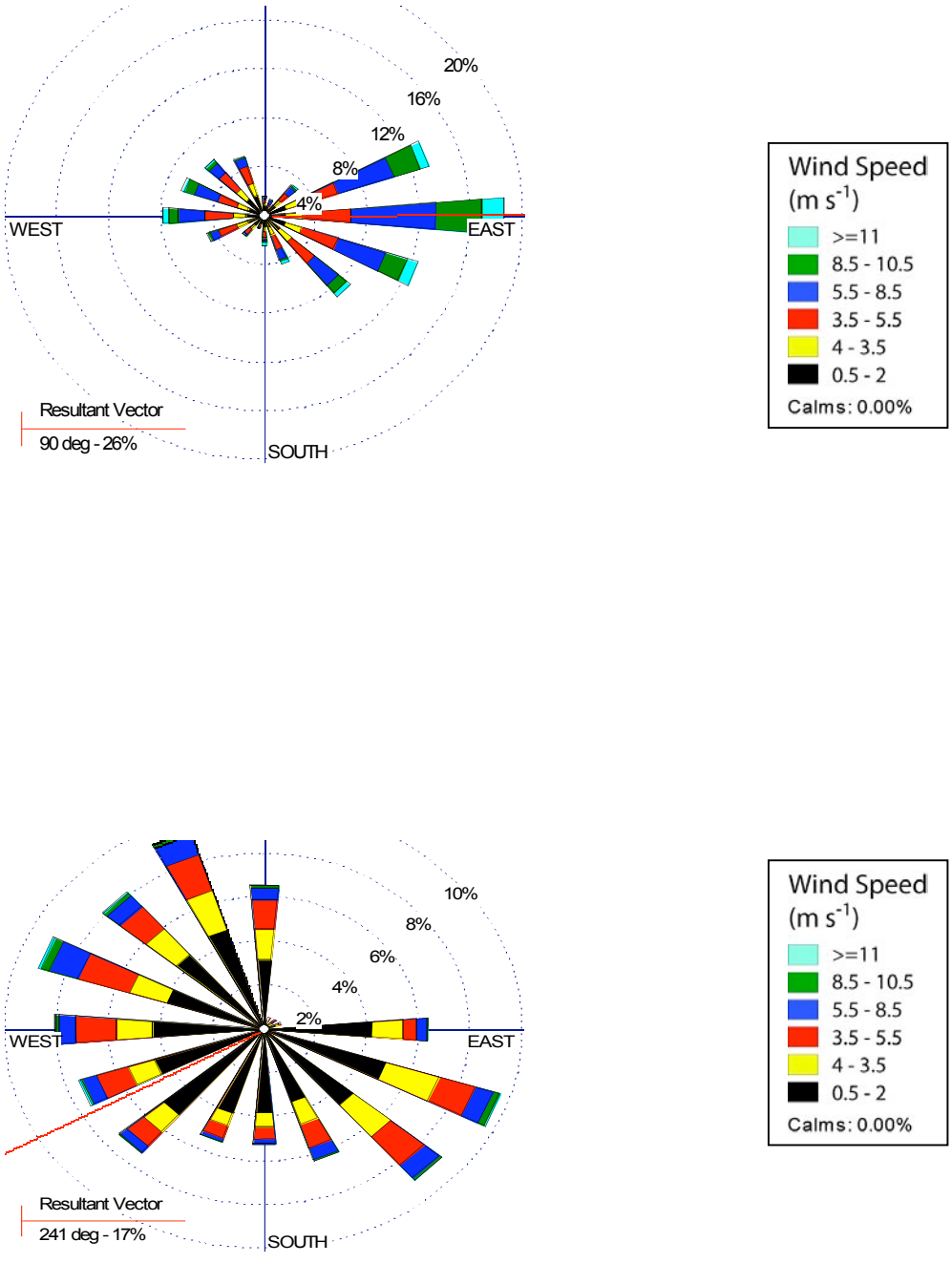

Fig. 23: Wind Rose for September; up: CFHT; below: UKIRT

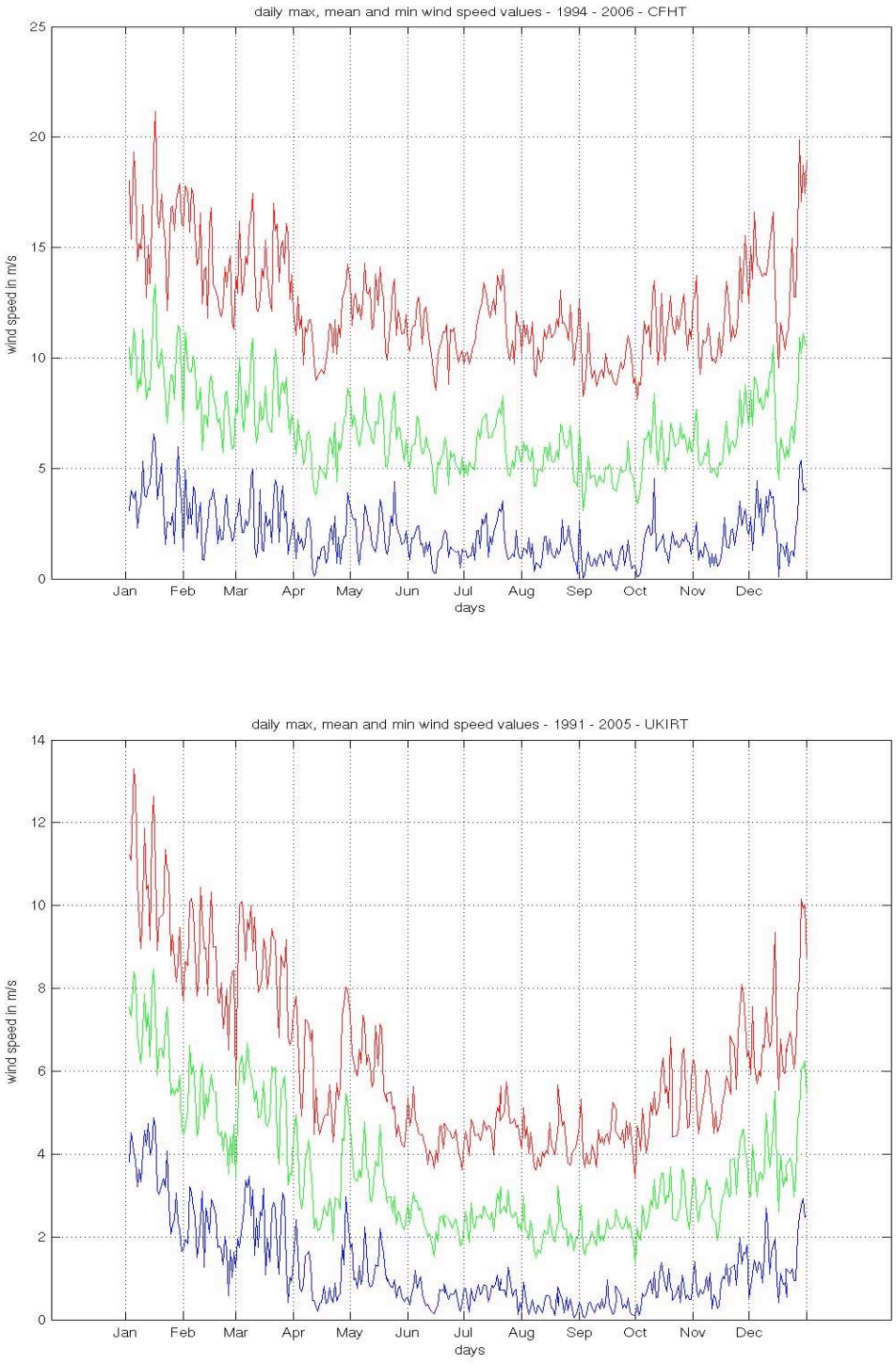

Fig. 24: Daily mean, mean of maximum and mean of minimum wind speed. Green line : wind speed mean along the year; red line : mean of maximum wind speed along the year; blue line : mean of minimum wind speed along the year.

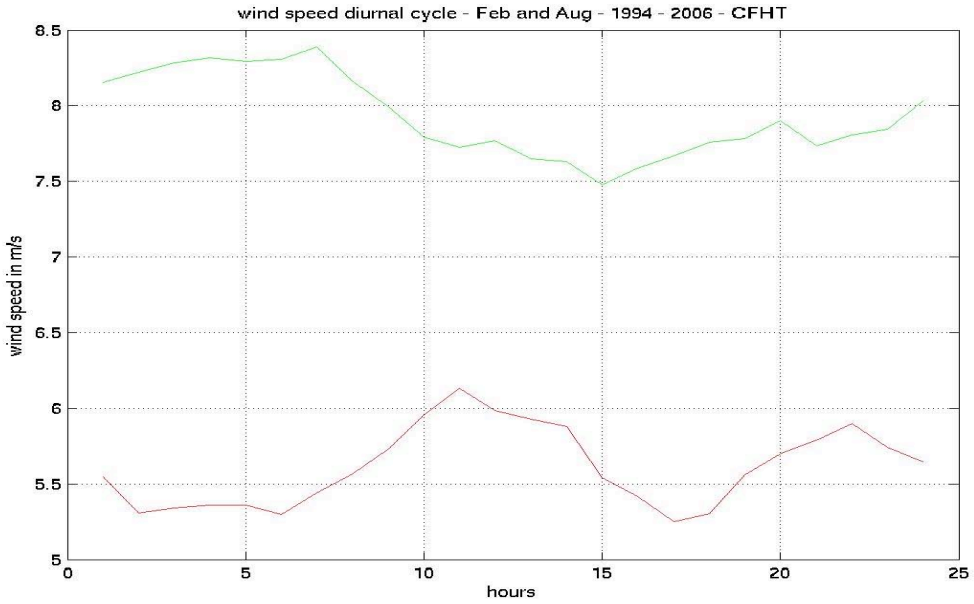

Fig. 25: Wind speed diurnal cycle. Green line: February; red line: August

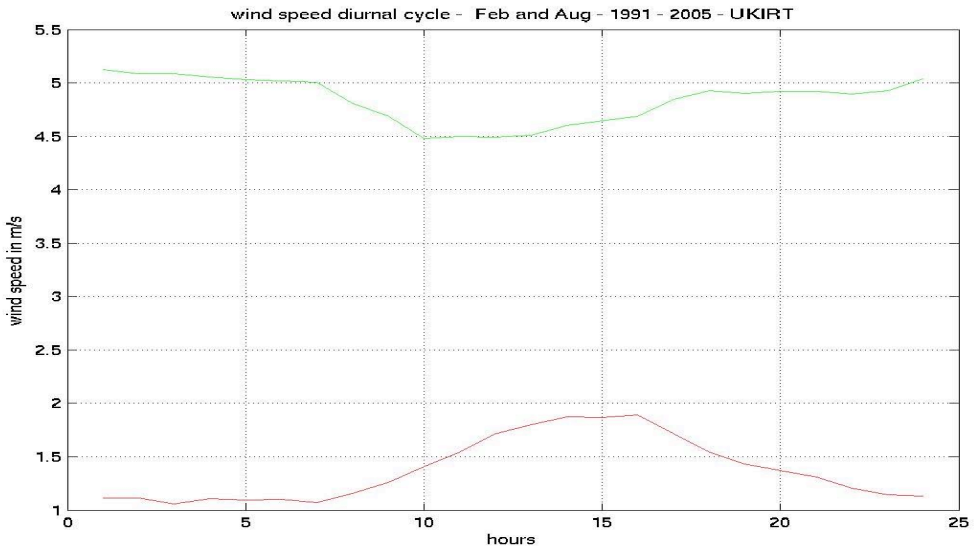

Fig. 25: Wind speed diurnal cycle. Green line: January; red line: August

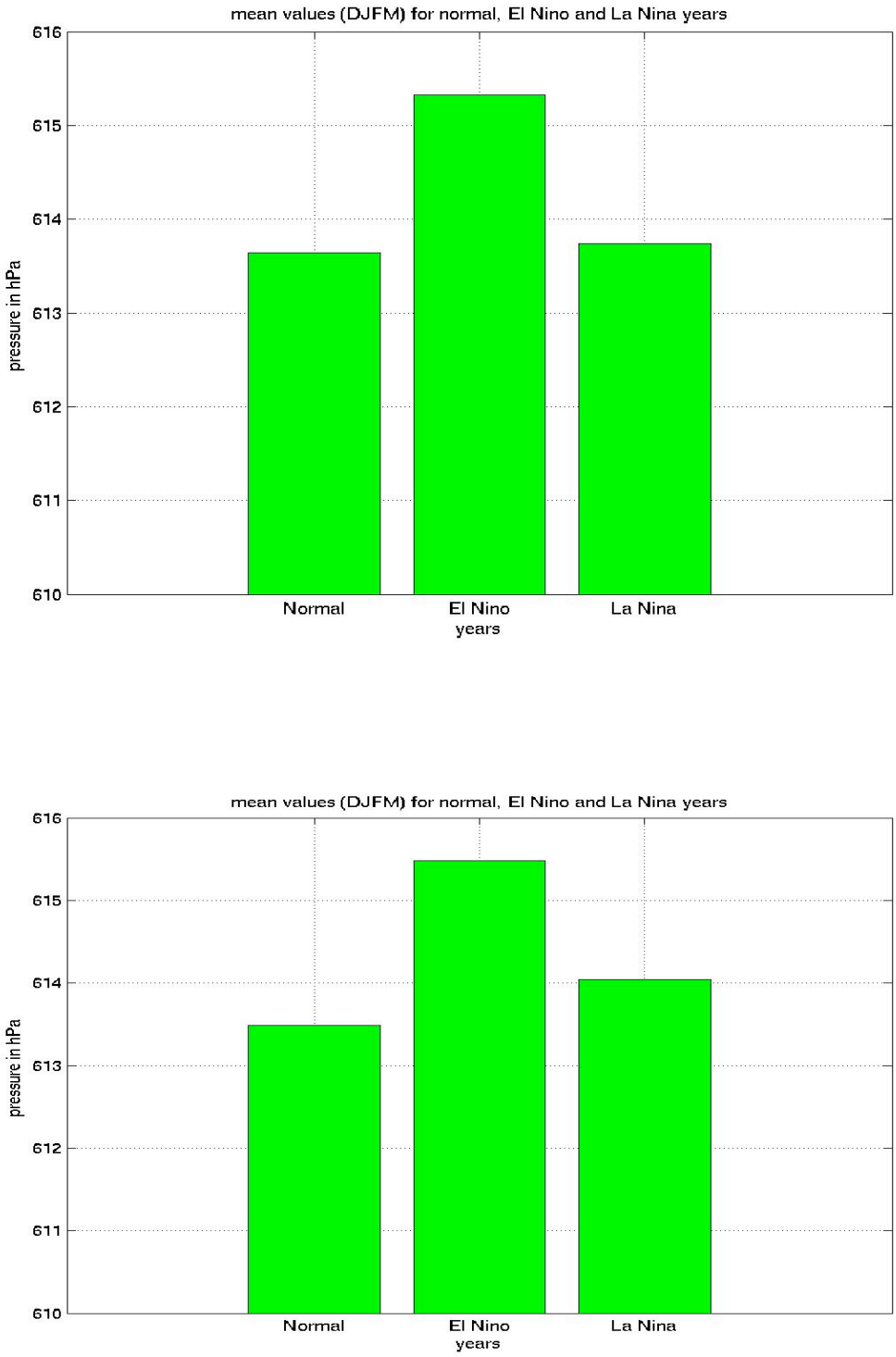

Fig. 26: Monthly mean bar plot for pressure for regular situation, El Niño and La Niña years, up: CFHT; below: UKIRT

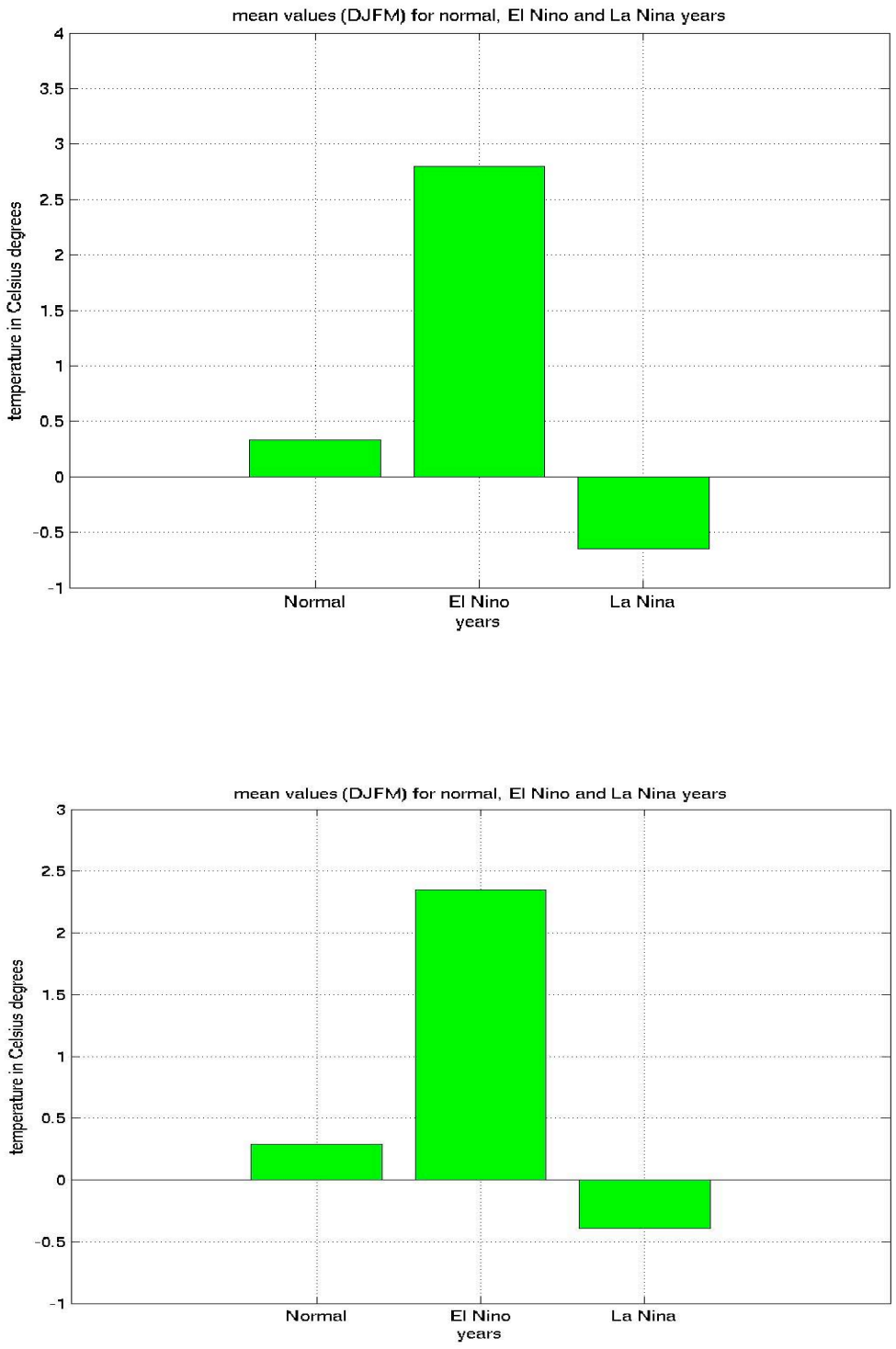

Fig. 27: Monthly mean bar plot for temperature for regular, El Niño and La Niña years; up: CFHT, below: UKIRT

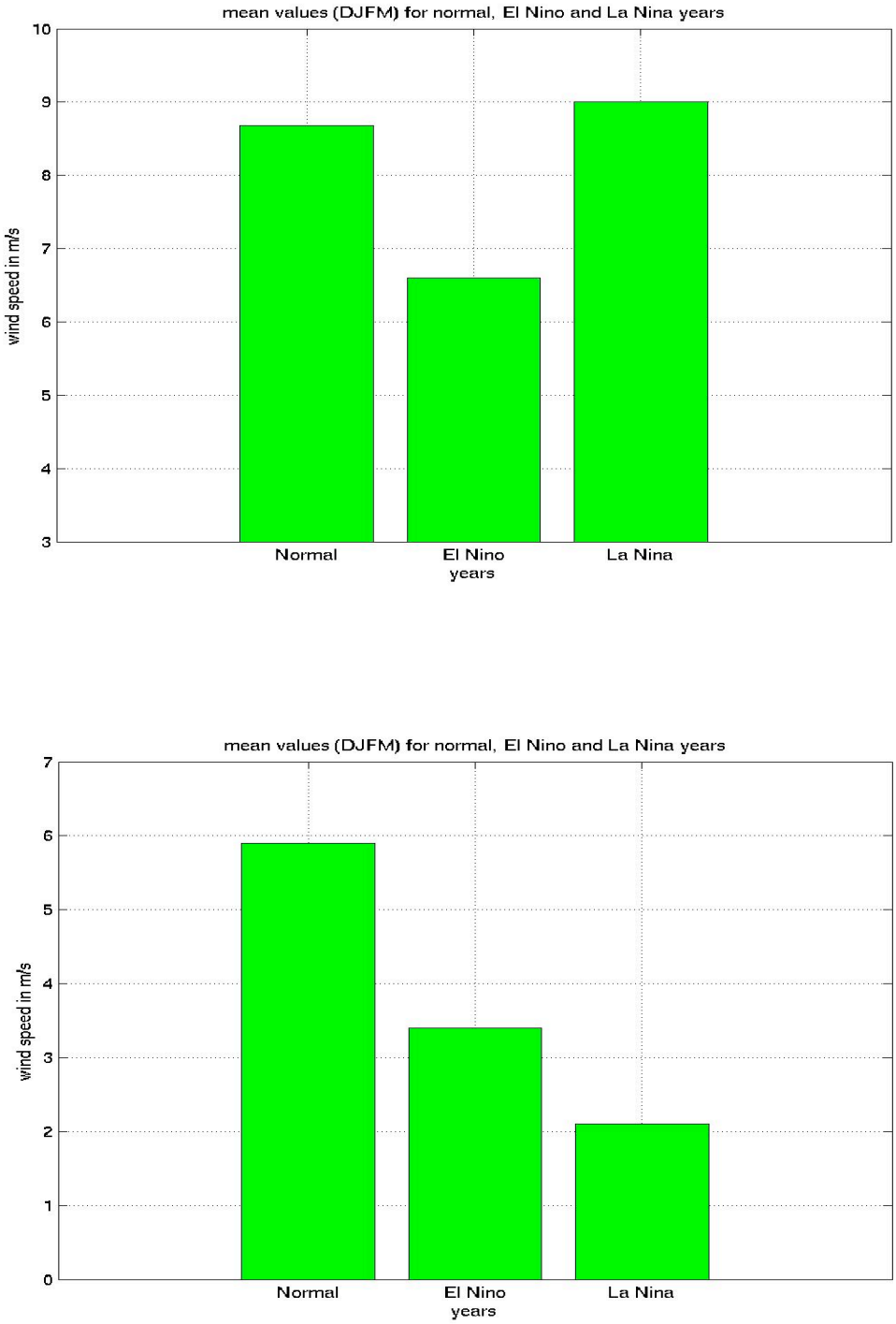

Fig. 28: Monthly mean bar plot for wind speed for regular, El Niño and La Niña years; up: CFHT, below: UKIRT

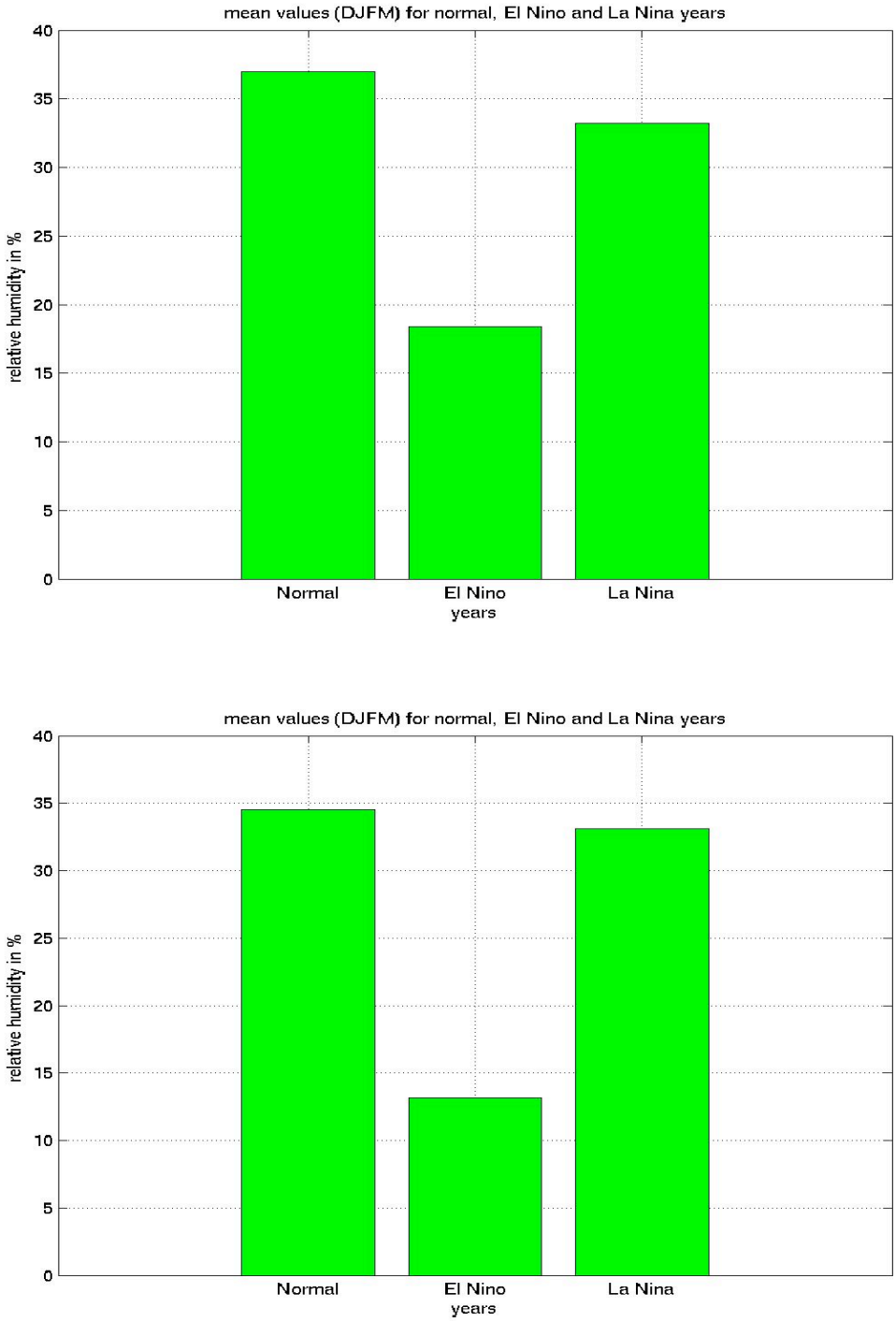

Fig. 29: Monthly mean bar plot for relative humidity for regular, El Niño and La Niña years; up: CFHT, below: UKIRT

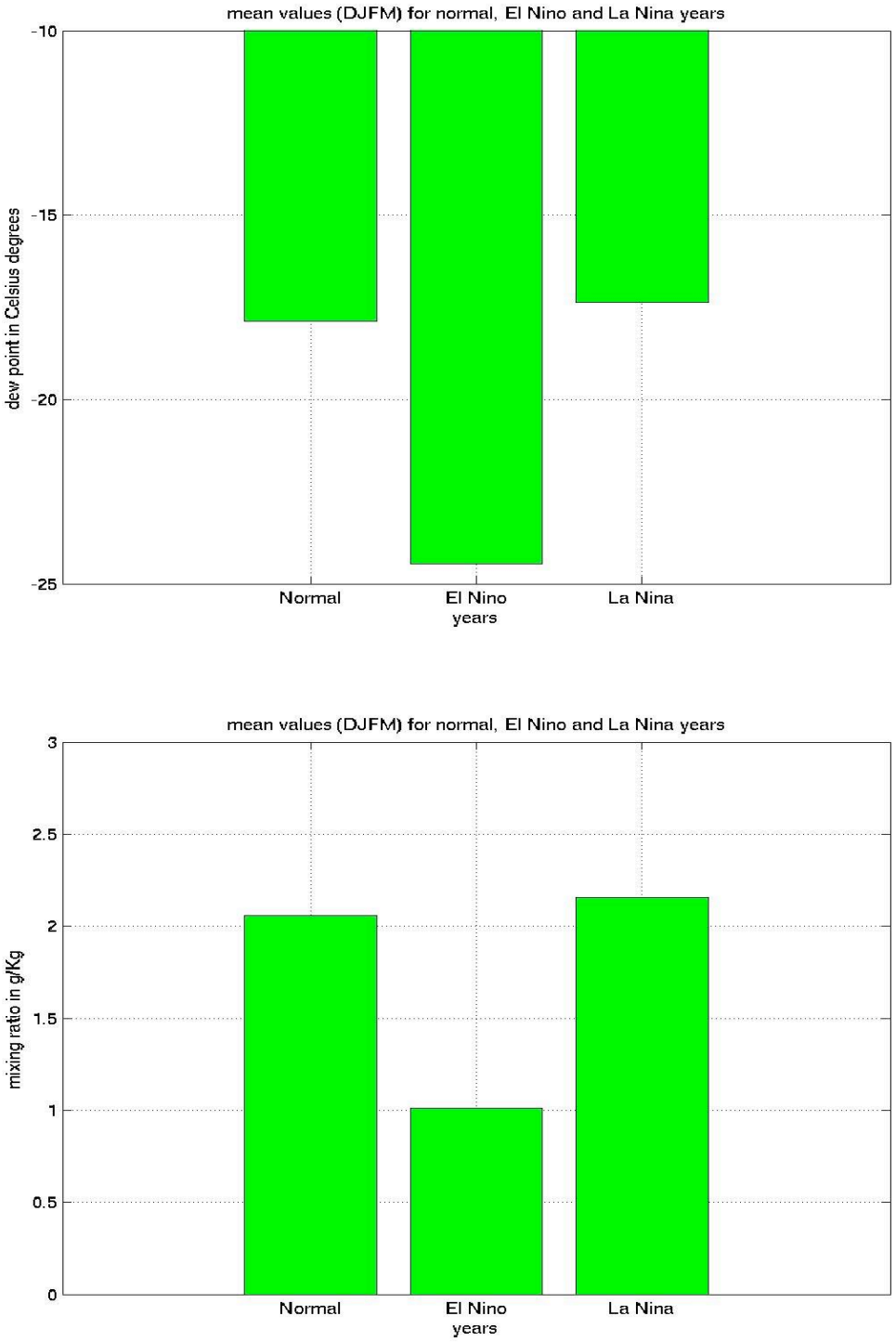

Fig. 30: Monthly mean bar plot for dew point (above) and mixing ratio (below) for regular, El Niño and La Niña years; up: CFHT, below: UKIRT

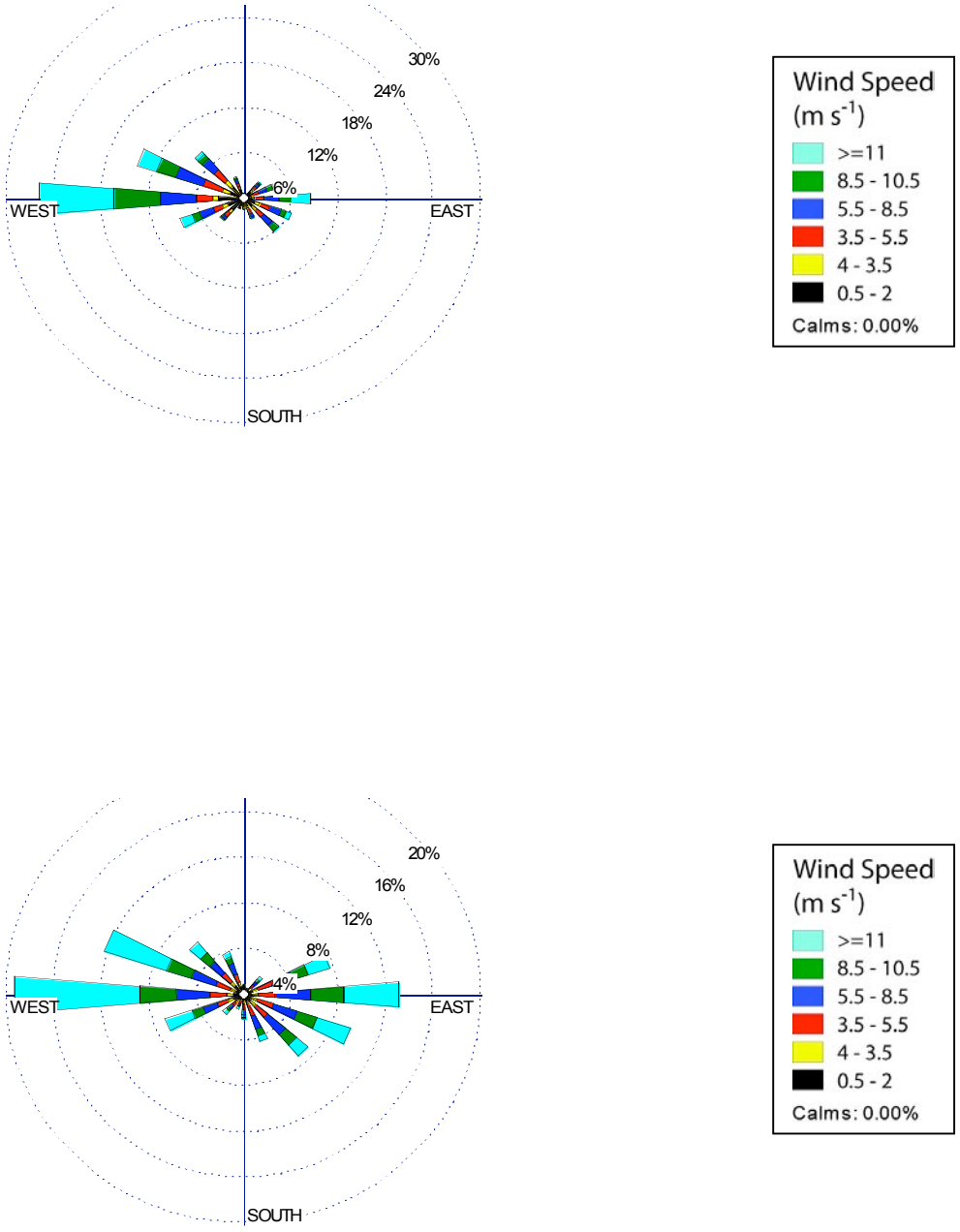

Fig. 31: Wind Rose plot for December, January, February and March for : above: El Niño year (Dec – 1997 and Jan, Feb and March – 1998); below : Normal situation (Dec – 1998 and Jan, Feb and March)

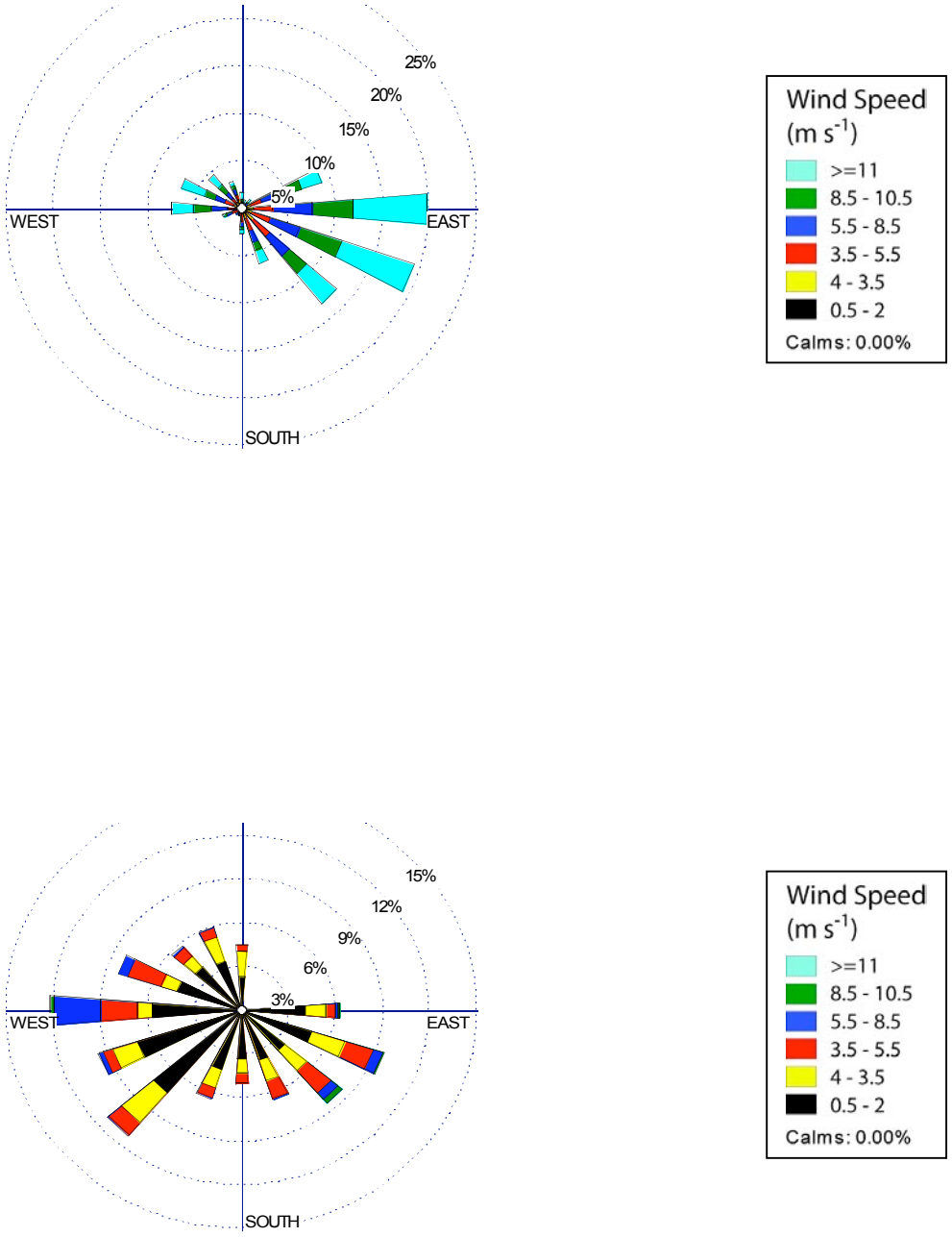

Fig. 32: Wind Rose for December, January, February and March of La Niña year (1998-99), up: CFHT; below: UKIRT

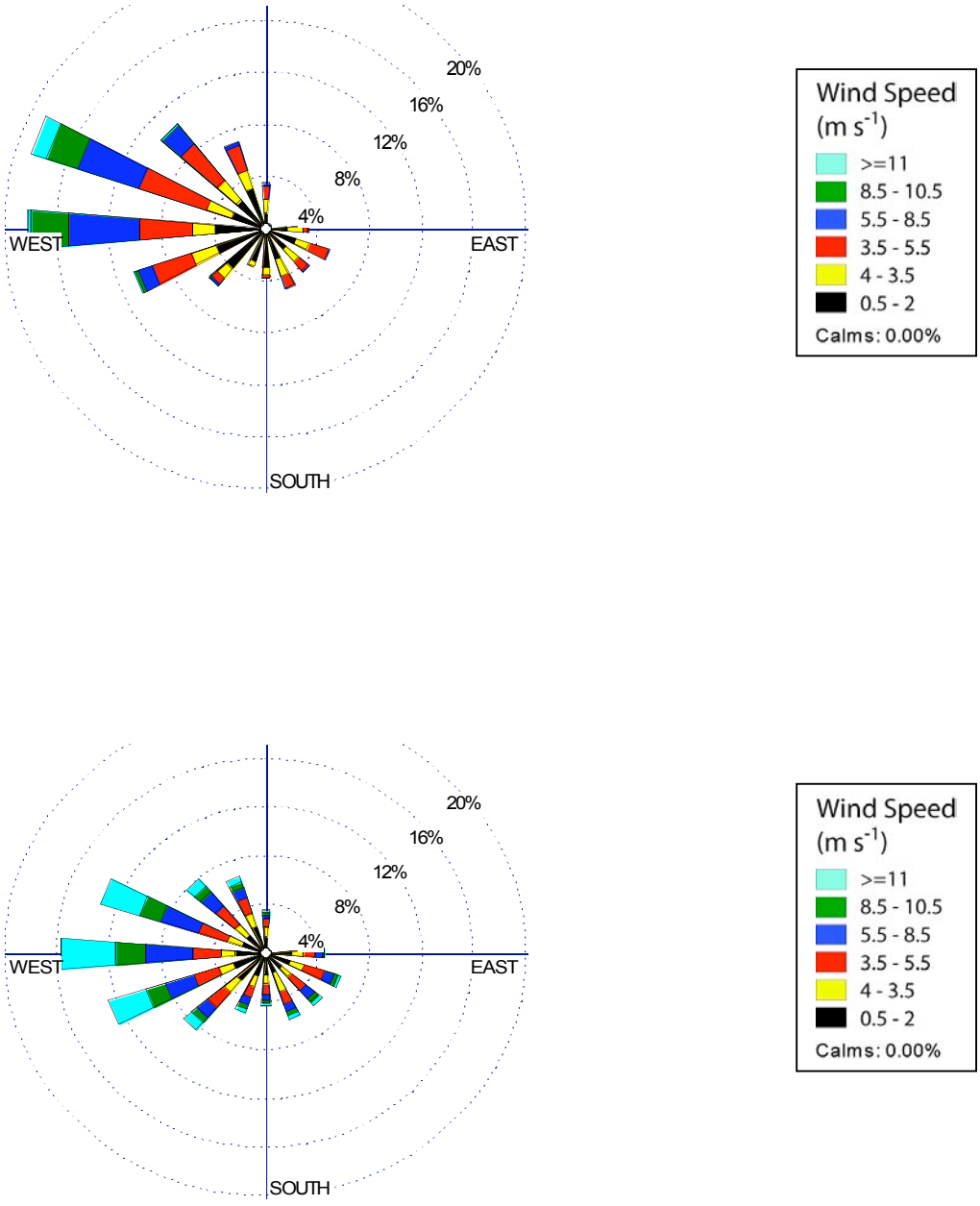

Fig. 33: Wind Rose for El Niño year (1997-1998) above and for regular situation below. – UKIRT

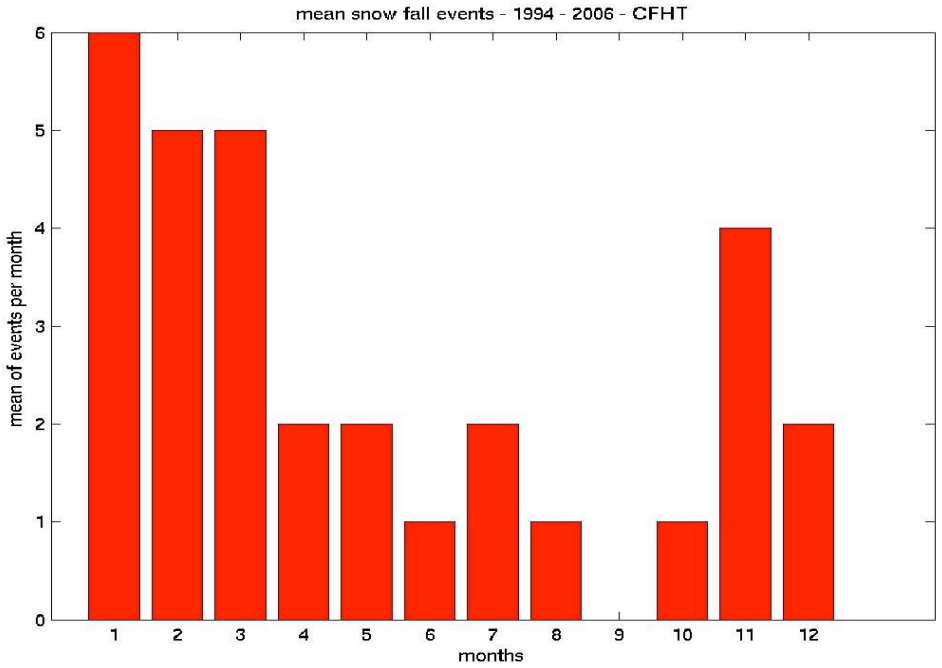

Fig. 34 a) Snowfall events proxy 1, CFHT

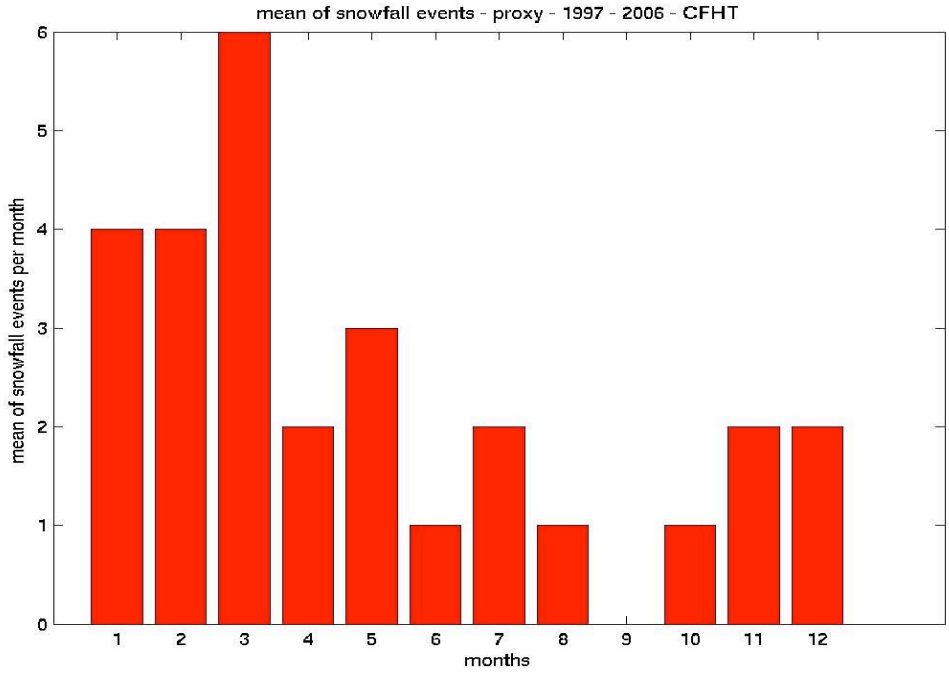

Fig. 34 b) Snowfall events proxy 2, CFHT

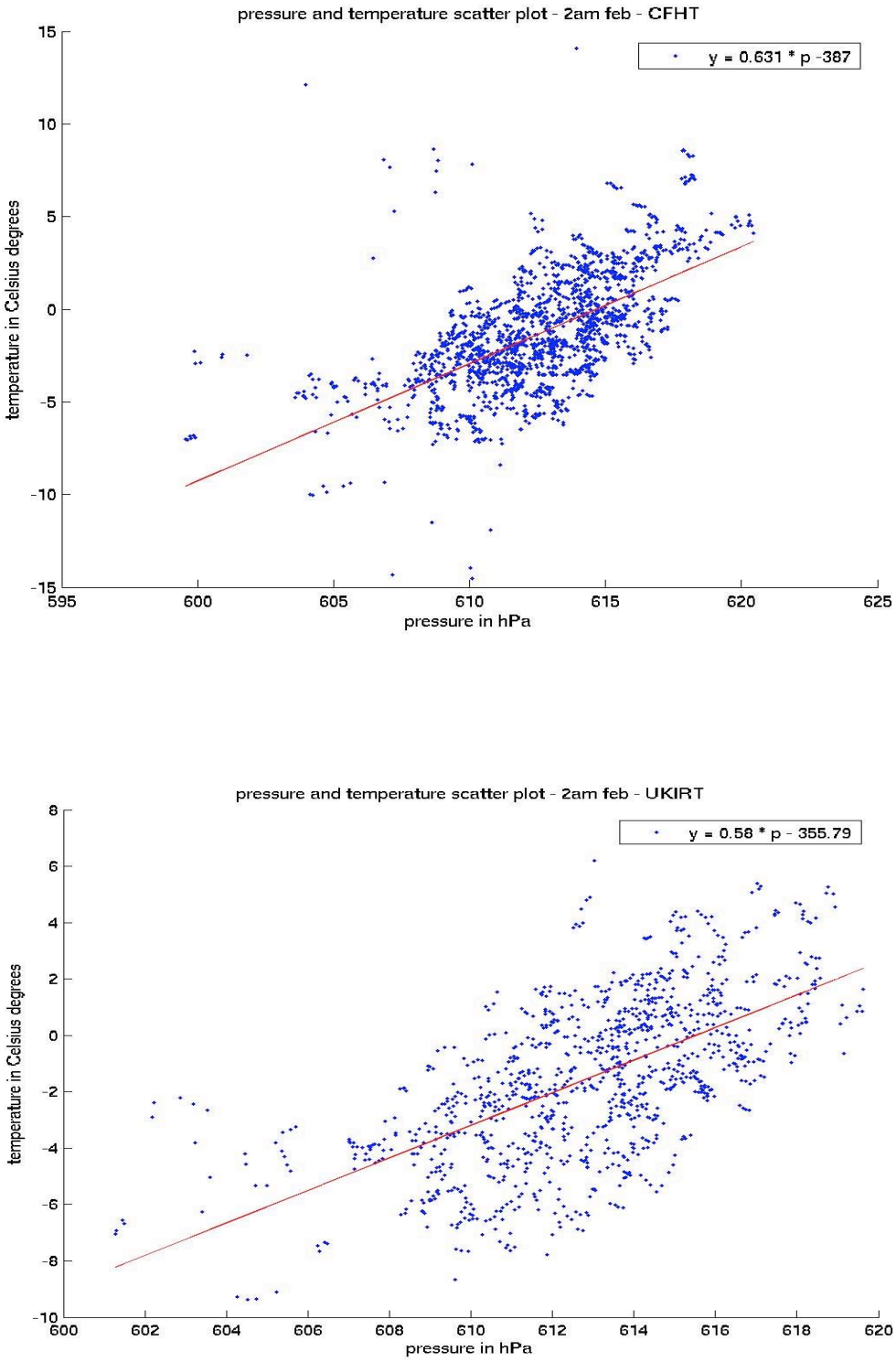

Fig. 35: Scatter plot to temperature as a response of pressure, for 2 am, February. Red line: robust fit line

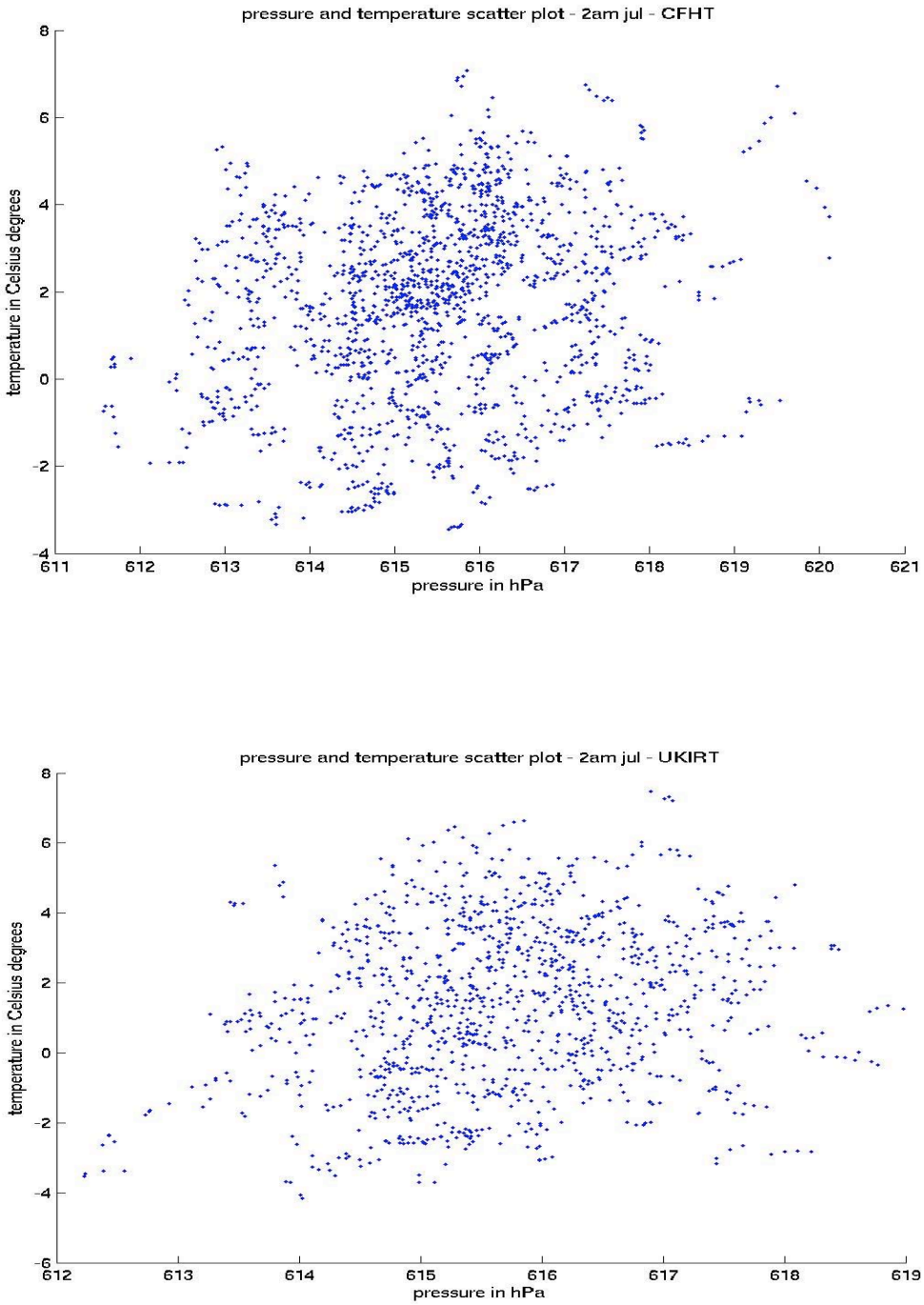

Fig. 36: Scatter plot for temperature as a response of pressure for 2 am, July.

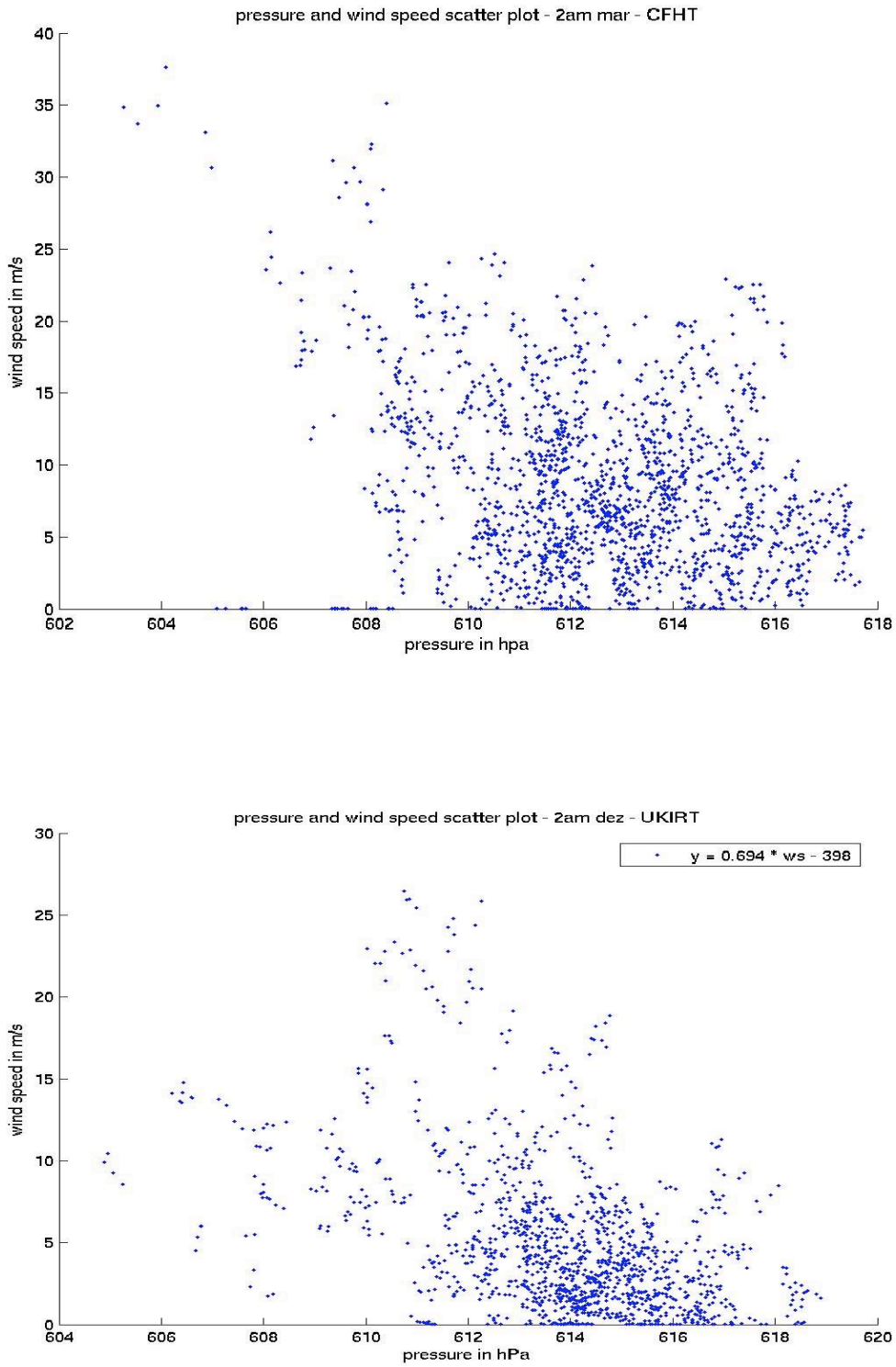

Fig. 37: Scatter plot for wind speed as a response of pressure for 2 am, above : March; below : December

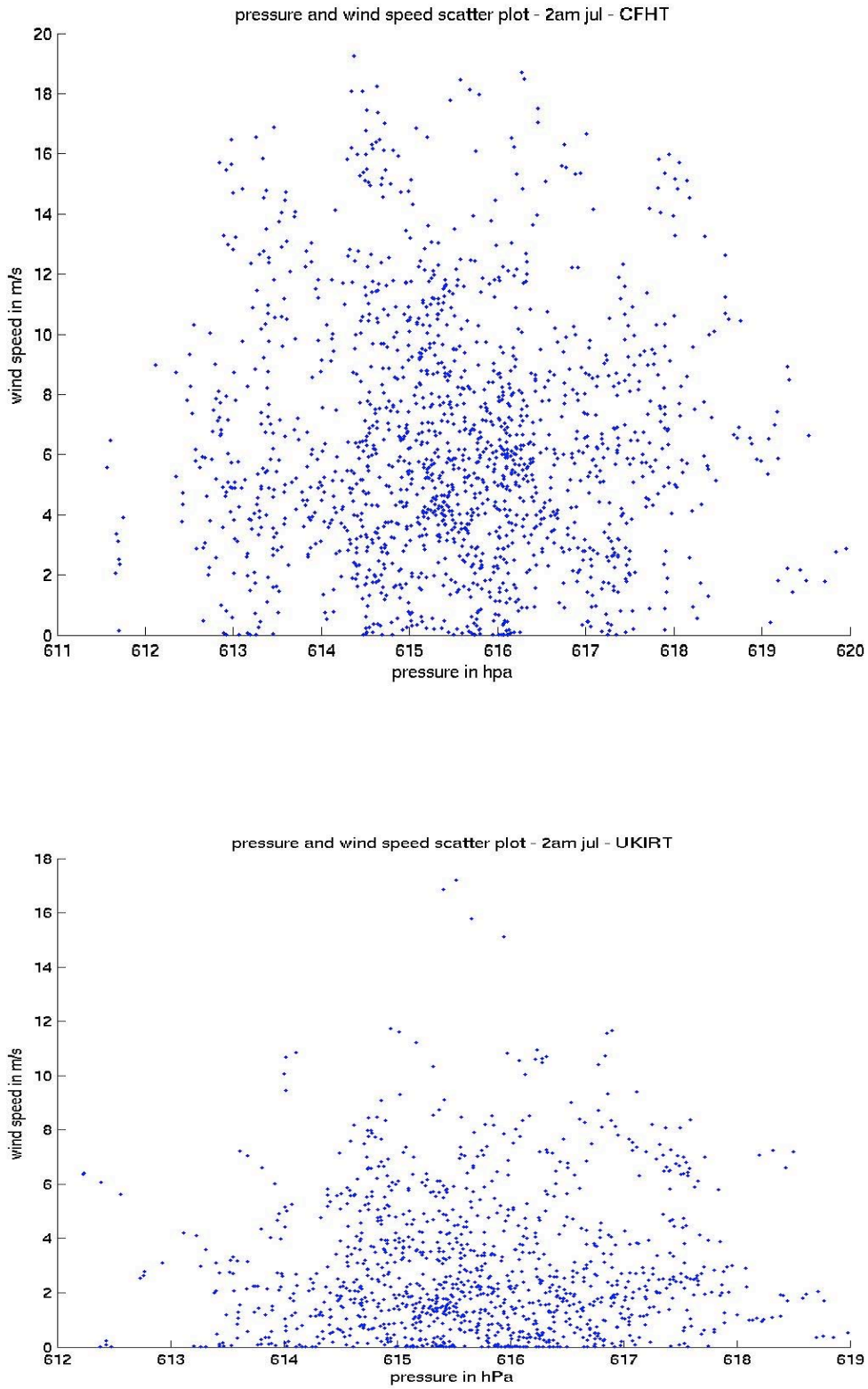

Fig. 38: Scatter plot for wind speed as a response of pressure, for 2 am, July

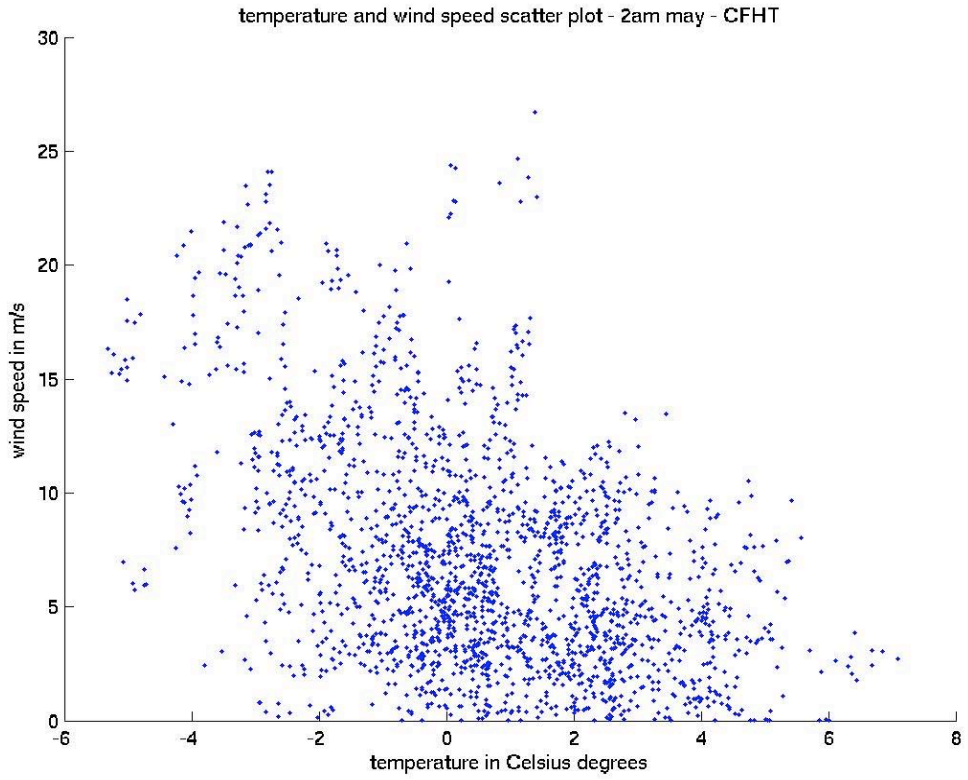

Fig. 39: Scatter plot for wind speed as a response of temperature, for 2 am, May, CFHT